Am J Cancer Res 2026;16(11):4709-4732
www.ajcr.us /ISSN:2156-6976/ajcr0175246

Original Article

An immune and metabolism-related gene signature for prognosis and *in vitro* functional analysis of CDH17 in lung adenocarcinoma

Jinfeng Lv[1,2,3], Ping Luo[1,2,3], Qianqian Ye[1,2,3], Shao Liu[1,2,3], Lan Fan[4,5]

[1]Department of Pharmacy, Xiangya Hospital, Central South University, Changsha 410008, Hunan, China; [2]National Clinical Research Center for Geriatric Diseases (Xiangya Hospital of Central South University), Changsha 410008, Hunan, China; [3]The Hunan Institute of Pharmacy Practice and Clinical Research, Changsha 410008, Hunan, China; [4]Department of Clinical Pharmacology, Xiangya Hospital, Central South University, Changsha 410078, Hunan, China; [5]Institute of Clinical Pharmacology, Central South University, Hunan Key Laboratory of Pharmacogenetics, Changsha 410078, Hunan, China

Received July 8, 2026; Accepted October 25, 2026; Epub November 15, 2026; Published November 30, 2026

Abstract: Tumor immunotherapy heterogeneity is increasingly recognized to be influenced by metabolic reprogramming and immune cell infiltration within the tumor microenvironment (TME). However, prognostic signatures integrating immune- and metabolism-related genes (IMRGs) for risk stratification and therapeutic response prediction in lung adenocarcinoma (LUAD) remain limited. We developed and validated a six-IMRGs prognostic signature in training and validation cohorts. The signature stratified LUAD patients into low-risk (LR) and high-risk (HR) groups, with significantly longer overall survival (OS) in the LR group. We also constructed a nomogram for individualized risk assessment. Single-sample gene set enrichment analysis (ssGSEA), immune checkpoint expression, immunophenoscore (IPS), and tumor immune dysfunction and exclusion (TIDE) analyses suggested that the LR group may benefit more from immunotherapy. Drug sensitivity analysis suggested that the HR group might be more sensitive to chemotherapy. These findings are exploratory and require further validation. Among the six IMRGs, CDH17 showed potential as an independent prognostic marker, but its functional role in LUAD remains poorly understood. Small interfering RNA (siRNA)-mediated silencing of CDH17 reduced LUAD cell proliferation and increased apoptosis. These findings provide preliminary insights into the role of CDH17 in LUAD and support further mechanistic and clinical studies.

Keywords: Lung adenocarcinoma, immune, metabolism, prognosis, tumor microenvironment, CDH17

Introduction

According to the latest 2024 global cancer statistics, lung cancer has surpassed other malignancies as the most commonly diagnosed cancer and the leading cause of cancer-related deaths worldwide in both sexes [1]. This malignancy is broadly classified into two main subtypes: non-small cell lung cancer (NSCLC) and small cell lung cancer (SCLC). Among NSCLC subtypes, lung adenocarcinoma (LUAD) and squamous cell carcinoma are the most prevalent, with LUAD accounting for approximately 40% of all NSCLC cases [2]. Early-stage LUAD is often asymptomatic, leading to late diagnosis in the majority of patients. The treatment for LUAD patients is stage-dependent, with surgical resection being the primary therapeutic approach for early-stage disease, whereas advanced-stage patients are limited to radiotherapy, chemotherapy, targeted therapy, or immunotherapy [3]. In recent years, immunotherapy has shown significant efficacy in LUAD. However, a substantial proportion of patients do not respond favorably to these treatments [4].

Emerging evidence suggests that heterogeneity in immunotherapy responses may stem from dynamic alterations within the tumor microenvironment (TME) [5, 6]. The TME comprises tumor cells, immune cells, endothelial cells, and extracellular matrix components, collectively foster-

https://doi.org/10.62347/SFGD9042

ing tumor growth, invasion, and metastasis [7]. Accumulating studies have indicated that the infiltration density, function and localization of immune cells within the TME significantly influence clinical outcomes in LUAD and other malignancies [8, 9]. Immune-related genes, particularly those encoding immune checkpoints such as PD-1 and PD-L1, modulate immune responses through interactions with cells in the TME. Immune checkpoint blockades (ICBs), by blocking PD-1/PD-L1, restore the antitumor activity of T cells, thereby achieving significant therapeutic effects in the treatment of LUAD [10, 11]. Additionally, metabolic alterations can suppress immune cell function and promote tumor progression [12, 13]. Given the critical interplay between immune regulation and metabolic reprogramming in cancer progression, prognostic models integrating immune- and metabolism-related genes (IMRGs) have been successfully applied in hepatocellular and colorectal carcinomas [14, 15]. However, to our knowledge, few IMRG-based prognostic signatures have been reported for LUAD. Thus, there is a need to develop IMRG-based prognostic tools for LUAD to facilitate risk stratification and provide clues for subsequent personalized therapeutic exploration.

In this study, we identified and validated a six-gene prognostic signature of IMRGs in LUAD, which showed significant correlations with patient survival and clinicopathological features. We constructed a predictive nomogram for individualized prognosis evaluation and analyzed the associations between risk scores and immune infiltration, tumor mutational burden (TMB), as well as chemotherapeutic sensitivity. Since our analysis revealed CDH17 as an independent prognostic factor in LUAD, and its expression pattern and biological roles have not been fully elucidated, we selected CDH17 from the signature genes for further experimental investigation. Cellular experiments revealed that small interfering RNA (siRNA)-mediated silencing of CDH17 inhibited proliferation and induced apoptosis in LUAD cells. Collectively, our findings suggest that CDH17 may serve as a candidate target for future investigations into LUAD therapy.

Material and methods

Data collection

We obtained LUAD transcriptomic profiles and clinical data from The Cancer Genome Atlas (TCGA, https://portal.gdc.cancer.gov) on 8 May 2023. The RNA-seq data included 503 tumor samples and 54 adjacent non-tumor samples. Patients with incomplete clinical data or survival time less than 30 days were excluded, yielding a final cohort of 448 LUAD cases with complete datasets. To ensure balanced distribution, patients were stratified by stage and age before random splitting using the createDataPartition function in R. Half of these samples were randomly selected as the internal validation cohort. Clinicopathological characteristics between the training and internal validation groups showed no statistically significant differences (Table S1). We constructed an external validation set using transcriptomic profiles of 439 LUAD patients (survival > 30 days) from the GSE68465 dataset of the Gene Expression Omnibus (GEO) database (https://www.ncbi.nlm.nih.gov/geo/). Prior to ComBat batch correction, gene expression data from both platforms were log2 transformed and standardized to Z scores across all samples. A list of 2483 immune-related genes was obtained from the ImmPort database (https://www.immport.org) [16] and 1723 metabolism-related genes were extracted from the Molecular Signature Database (https://www.gsea-msigdb.org) [17]. We merged the two gene lists and obtained 1063 overlapping genes defined as IMRGs. Among them, 906 IMRGs had corresponding mRNA expression data present in both the TCGA and GEO datasets.

Identification of differentially expressed IMRGs

Differential expression analysis between LUAD and adjacent non-tumor tissues was conducted using the “limma” R package [18]. Differentially expressed genes were identified with thresholds of adjusted *P*-value (FDR) < 0.05 and |log2FC| > 0.5.

Prognostic signature construction and validation

We performed a least absolute shrinkage and selection operator (LASSO) Cox regression using the “glmnet” R package to establish a prognostic signature [19]. Patients within the TCGA training cohort were stratified into low-risk (LR) and high-risk (HR) groups based on median risk scores. This stratification threshold was subsequently applied to internal and external validation cohorts. Associations between risk scores and clinicopathological parameters (gender,

age, stage and TNM) were evaluated. Prognostic performance was assessed using Kaplan-Meier survival analysis and time-dependent receiver operating characteristic (ROC) curves for overall survival (OS).

Prognostic nomogram construction and validation

A multivariate nomogram integrating the IMRGs signature and clinical parameter was constructed to predict patient survival probabilities. Calibration curves, ROC analyses, and decision curve analysis (DCA) were used to evaluate the accuracy of the nomogram and its clinical utility.

Functional enrichment analyses

Gene Set Enrichment Analysis (GSEA) version 4.3.3 (https://www.broadinstitute.org/gsea/index.jsp) was applied to identify enriched biological functions and pathways between LR and HR groups using Gene Ontology (GO) and Kyoto Encyclopedia of Genes and Genomes (KEGG) gene sets [20].

Immune infiltration analysis

ESTIMATE score, immune score, stromal score and tumor purity were calculated using the "ESTIMATE" R package [21]. Immune cell infiltration profiles were analyzed via Single-sample Gene Set Enrichment Analysis (ssGSEA) [22].

Immunotherapy response prediction

Differential expression of 48 immune checkpoint genes was evaluated between the LR and HR groups. Immunophenoscore (IPS; https://tcia.at) [23] and Tumor Immune Dysfunction and Exclusion (TIDE; http://tide.dfci.harvard.edu) [24] algorithms were used to further investigate the predictive potential of the IMRGs prognostic signature for immunotherapy efficacy. TMB was calculated from somatic mutation data, and waterfall plots of somatic mutations were generated with the "maftools" R package.

Tumor stemness correlation

The stemness properties of tumors can be measured with RNA stemness score based on mRNA expression (RNAss) and DNA stemness score based on DNA methylation (DNAss) [25]. Spearman correlation analysis was used to investigate the association between the risk scores and both the RNAss and the DNAss.

Chemotherapeutic sensitivity profiling

We used the "pRRophetic" R package to predict the half-maximal inhibitory concentrations (IC_{50}) [26, 27] of common chemotherapeutic agents.

Cell culture and transfection

A549 and H1299 human lung adenocarcinoma cell lines were purchased from the Cell Bank of the Chinese Academy of Sciences (Shanghai, China). The human normal bronchial epithelial cell line BEAS-2B was purchased from Abiowell (Changsha, China). All cell lines were routinely tested for mycoplasma contamination and authenticated by STR profiling. H1299 and BEAS-2B cells were cultured in RPMI-1640 medium (Abiowell, AW-M018, China), and A549 cells were grown in DMEM (Abiowell, AW-M003, China). Both media were supplemented with 10% fetal bovine serum (FBS) and 1% penicillin-streptomycin. All cells were maintained at 37°C under a humidified incubator with 5% CO_2. The function of CDH17 in these lung adenocarcinoma cell lines was examined by knocking down CDH17 expression using siRNA transfection in the cell line with relatively higher CDH17 expression. Prior to transfection, H1299 cells were seeded in 6-well plates and grown to 50%-60% confluence. Cell transfection was performed with 100 nM siRNA and Lipofectamine 2000 (Invitrogen, Thermo Fisher Scientific, Shanghai, China). The silencing effect of CDH17 was analyzed by real-time quantitative PCR (RT-qPCR) and Western blot to detect the expression level of CDH17 in H1299 cells. The sequences of synthesized siRNAs are presented in **Table 1**. After 48 h of transfection, cells were used for further experiments.

RT-qPCR

Total RNA was extracted from cultured cells using TRIzol reagent (Invitrogen, USA). Reverse transcription was performed with a reverse transcription kit (CW2569, CWBIO, China) at 50°C for 50 min and 85°C for 5 min. Quantitative PCR was carried out on an ABI-QS1 quantitative PCR instrument (Applied Biosystems, Thermo Fisher Scientific, USA). A 30 μL

Table 1. Sequences of siRNA used in this study

Name	Sequences
si-CDH17-905	Sense: 5'-CAA AGG AUG AGU ACG GAA ATT-3'
	Antisense: 5'-UUU CCG UAC UCA UCC UUU GTT-3'
si-CDH17-935	Sense: 5'-CAU AUC CGC UGG AAA UUC ATT-3'
	Antisense: 5'-UGA AUU UCC AGC GGA UAU GTT-3'
si-CDH17-962	Sense: 5'-AAA AGG AUG CAG UGA GUA ATT-3'
	Antisense: 5'-UUA CUC ACU GCA UCC UUU UTT-3'
si-NC	Sense: 5'-UUC UCC GAA CGU GUC ACG UTT-3'
	Antisense: 5'-ACG UGA CAC GUU CGG AGA ATT-3'

master mix was prepared for each sample, containing 15 μL 2×SYBR Green PCR Master Mix, 1 μL forward primer (10 μM), 1 μL reverse primer (10 μM), 2 μL cDNA, and 11 μL ddH_2O. Then, 10 μL of this mixture was aliquoted into each of three replicate wells. The amplification protocol was 95°C for 10 min, followed by 40 cycles of 95°C for 15 s and 60°C for 30 s, with melting curve analysis from 60°C to 95°C. Relative mRNA levels were calculated using the $2^{-\Delta\Delta CT}$ method with β-actin as the internal reference. The primer sequences (5'-3') were as follows: CDH17-F: TTGTCTGATTGGGGCTCCTG; CDH17-R: GACTCGGTTCTTGGCCTTCA; β-actin-F: ACCCTGAAGTACCCCATCGAG; β-actin-R: AGCACAGCCTGGATAGCAAC.

Western blotting

Total cellular proteins were extracted from cells using RIPA lysis buffer, and the protein concentration was determined using the bicinchoninic acid (BCA) assay. The same amount of protein and molecular weight standard were sampled into SDS-PAGE gel well, and electrophoresis was performed at 75 V for 130 min. The proteins were subsequently transferred onto nitrocellulose (NC) membranes at 300 mA for 2 h for CDH17 (120 kDa) and for 60 min for β-actin (42 kDa). After transfer, the membranes were blocked with a sealing buffer for 90 min at room temperature and then incubated overnight at 4°C with primary antibodies against CDH17 and β-actin (diluted at 1:5000; Proteintech). After three washes with PBST, the membranes were incubated with HRP-conjugated secondary antibodies (diluted at 1:5000; Abiowell) for 90 min at room temperature. The protein bands were visualized using enhanced chemiluminescence (ECL). β-actin served as the internal reference.

Cell proliferation assay

The proliferation abilities of H1299 cells after transfection were quantitatively assessed using the Cell Counting Kit-8 (CCK-8) assay. Following 48 h of intervention, 10 μL CCK-8 solution was supplemented into each 100 μL complete culture medium, and cells were further incubated at 37°C under a humidified atmosphere with 5% CO_2 for an additional 4 h. The absorbance value (OD_{450}) was sequentially measured at 0 h, 24 h, 48 h and 72 h via a HEALES MB-530 microplate spectrophotometer.

Flow cytometry analysis of apoptosis

After transfection, H1299 cells were seeded in 6-well plates. The cells were harvested by trypsinization, washed twice with 5 mL of phosphate-buffered saline (PBS), and resuspended in 500 μL of binding buffer. The cell suspension was incubated with 5 μL of Annexin V-allophycocyanin (APC) and 5 μL of propidium iodide (PI) staining solution at room temperature in the dark. Apoptosis was then analyzed by flow cytometry, with approximately 10,000 events (range: 9 701-11 785) acquired per sample. Early apoptotic cells were defined as Annexin V+/PI- (Q3), late apoptotic cells as Annexin V+/PI+ (Q2), necrotic cells as Annexin V-/PI+ (Q1), and viable cells as Annexin V-/PI- (Q4). The apoptosis rate was calculated as the sum of the percentages of early-apoptotic (Q3) and late-apoptotic (Q2) cell populations.

Cell colony formation experiment

The transfected H1299 cells were reseeded for colony formation assays 48 h after siRNA transfection, when CDH17 knockdown had been validated. Cells (2×10^2 cells/well) were seeded into six-well plates, and cultured for 14 days. Cells were then fixed with 4% paraformaldehyde, washed twice with PBS, and stained with 1 mL crystal violet for 30 min.

Statistical analysis

Statistical analyses were conducted using R software 4.2.3 and GraphPad Prism 11.0.0. For comparisons between two groups, an unpaired t-test with Welch's correction was

used for normally distributed data, while the Mann-Whitney U test (non-parametric) was applied when normality was not met. Time-course data were analyzed by two-way repeated-measures ANOVA. For multi-group comparisons among three or more groups, one-way ANOVA followed by Tukey's post-hoc test was used for parametric data, whereas the Kruskal-Wallis test followed by Dunn's test with multiple-comparison correction was adopted for non-parametric data. Kaplan-Meier analysis and Log-Rank test were applied to survival assessment, and correlations were quantified using Spearman's method. Statistical significance was set at $P < 0.05$. All *in vitro* experiments were performed in three independent biological replicates. Data are presented as mean ± SD.

Results

Identification of differentially expressed IMRGs in LUAD patients

The bioinformatics analyses are summarized in **Figure 1**. Through integration of mRNA-sequencing data from the TCGA and GEO databases, 906 IMRGs were initially identified. Subsequent differential expression analysis between tumor and adjacent normal tissues revealed 66 significantly altered IMRGs, comprising 30 downregulated and 36 upregulated genes (**Figure 2A**).

Construction of an IMRG-based prognostic signature for LUAD

Univariate Cox regression analysis identified 30 differentially expressed IMRGs significantly associated with prognosis ($P < 0.05$; Table S2). To refine prognostic biomarkers, LASSO regression and multivariate Cox proportional hazards analysis were performed, yielding six genes with independent prognostic value (**Figure 2B-D**). A prognostic risk score model was established using the formula: Risk score = (0.173544*ASPM expression) + (0.259986*PLEK2 expression) + (0.132416*FERMT1 expression) + (-0.109960*MAOB expression) + (-0.184446*PLA2G3 expression) + (0.099374*CDH17 expression). Based on the median risk score, LUAD patients in the TCGA training cohort were stratified into LR and HR groups to assess prognostic relevance.

Validation of the IMRGs prognostic signature

In the TCGA training cohort, Kaplan-Meier survival analysis showed significantly longer OS in the LR group than in the HR group ($P < 0.001$; **Figure 3A**). Higher risk scores were associated with a greater proportion of deceased patients (**Figure 3B**, **3C**). Heatmap analysis revealed that PLA2G3 and MAOB were elevated in the LR group, whereas ASPM, PLEK2, FERMT1, and CDH17 were elevated in the HR group (**Figure 3D**). In ROC analysis, the risk score showed better prognostic performance than conventional clinical parameters (**Figure 3E**). The time-dependent ROC analysis yielded area under the curve (AUC) values of 0.759 (95% CI: 0.679-0.824), 0.674 (95% CI: 0.604-0.751), and 0.671 (95% CI: 0.589-0.771) for 1-, 3-, and 5-year survival, respectively (**Figure 3F**). Consistent results were obtained in internal (TCGA validation cohort; Figure S1A-C) and external validation cohorts (GEO datasets; Figure S1D-F), supporting the generalizability of the signature.

Association of the IMRGs prognostic signature with clinicopathological features

To validate the clinical prognostic utility of the IMRGs risk stratification model in LUAD, we analyzed its correlation with key clinicopathological parameters (gender, age, stage, TNM) in the TCGA-LUAD cohort. Kaplan-Meier survival analysis showed that the LR group had significantly longer OS than the HR group in each stratified subgroup: gender (female: $P < 0.001$; male: $P < 0.001$; **Figure 4A**, **4B**), age (< 65: $P < 0.001$; ≥ 65: $P < 0.001$; **Figure 4C**, **4D**), stage (I-II: $P < 0.001$; III-IV: $P = 0.005$; **Figure 4E**, **4F**), T (T1-2: $P < 0.001$; T3-4: $P < 0.001$; **Figure 4G**, **4H**), N (N0: $P < 0.001$; N1-3: $P = 0.016$; **Figure 4I**, **4J**), and M (M0-1: $P < 0.001$; **Figure 4K**). Higher risk scores were associated with male gender ($P < 0.01$), advanced-stage (III-IV; $P < 0.01$), higher T (T3-4; $P < 0.05$) and higher N (N1-3; $P < 0.001$) (Figure S2), suggesting that the LR group tended to show less aggressive tumor progression and a lower prevalence of advanced disease than the HR group.

Comparative performance evaluation against established prognostic signatures

To evaluate the predictive capacity of our IMRGs signature, we compared it with four pub-

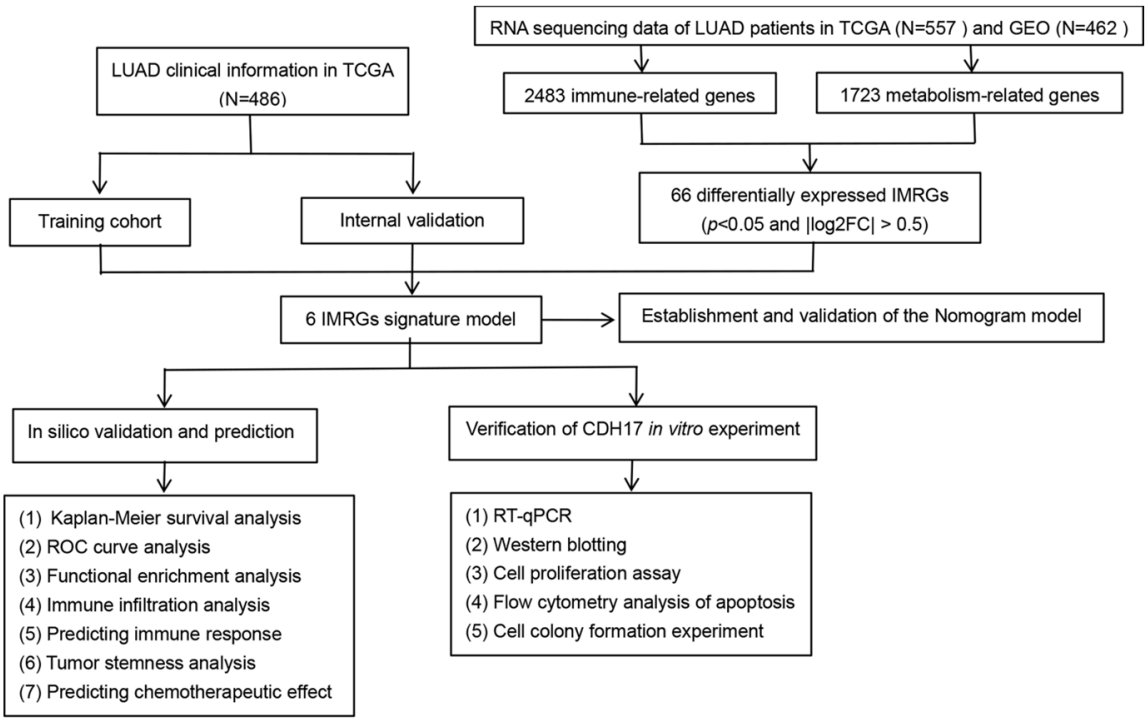


Figure 1. The flow diagram of the present study. LUAD, lung adenocarcinoma; TCGA, The Cancer Genome Atlas; GEO, Gene Expression Omnibus; IMRGs, immune- and metabolism-related genes; FC, fold change; ROC, receiver operating characteristic; RT-qPCR, real-time quantitative PCR.

lished LUAD prognostic models: Chang signature [28] (a three-gene model), Chen signature [29] (a sixteen-gene model), Jiang signature [30] (a six-gene model) and Tang signature [31] (a four-gene model). To ensure comparability, the same method was applied to calculate and convert the risk scores for the entire TCGA-LUAD dataset. All models stratified patients into LR and HR groups with distinct survival outcomes (**Figure 5A-D**). Compared with these models, the IMRG signature showed higher time-dependent AUC values for 1-, 3-, and 5-year survival (**Figures 3F**, **5E-H**). The C-index of the IMRG signature (0.663) was higher than that of the Chang (0.582), Chen (0.632), Jiang (0.644), and Tang (0.641) signatures (**Figure 5I**).

Development and validation of a prognostic nomogram integrating IMRGs signature

Univariate Cox regression showed that the stage, T/N/M, and IMRGs risk score were significantly associated with OS (**Figure 6A**). Multivariate analysis further suggested that stage and risk score were independent prognostic predictors for LUAD patients (**Figure 6B**). These findings were consistent in the internal and external validation cohorts (Figure S3). A nomogram integrating the IMRGs risk score and stage was developed to predict 1-, 3-, and 5-year OS probabilities (**Figure 6C**). Calibration plots showed good concordance between predicted and observed survival outcomes (**Figure 6D**). The nomogram showed higher predictive accuracy (AUC: 0.827 (95% CI: 0.762-0.896), 0.759 (95% CI: 0.702-0.823), and 0.769 (95% CI: 0.675-0.851) for 1-, 3-, and 5-year OS, respectively) than individual prognostic factors (**Figure 6E-G**). Decision curve analysis (DCA) indicated that the nomogram achieved the highest net benefit over a broader range of threshold probabilities than the other parameters (**Figure 6H-J**).

Functional enrichment analysis

Functional enrichment analysis suggested distinct biological processes between the LR and HR groups. GO enrichment analysis revealed that the HR group was enriched in the mitotic nuclear division, microtubule organization in mitosis, organelle fission, and chromosome condensation and localization. The LR group

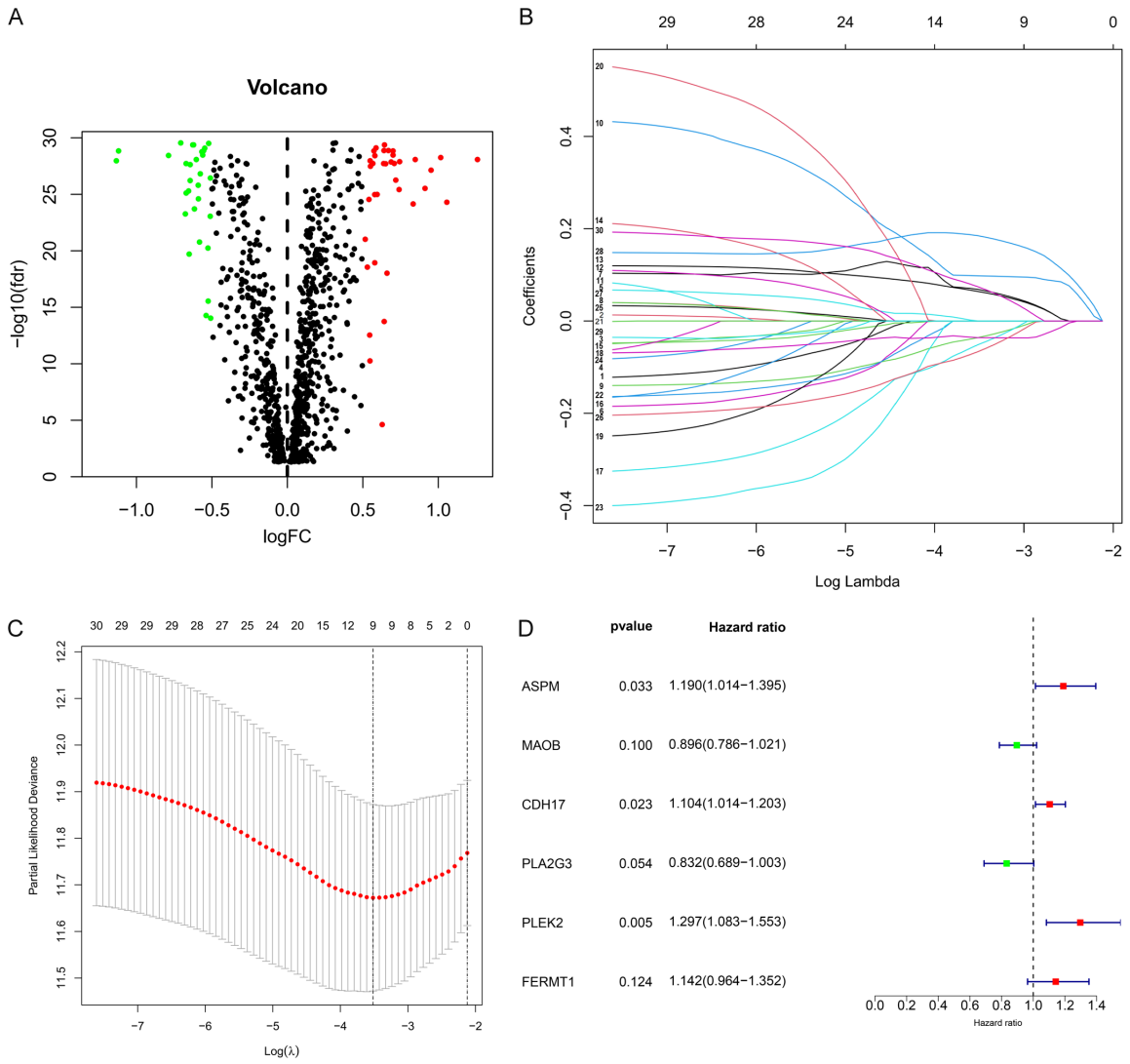


Figure 2. Construction of a prognostic signature based on differentially expressed IMRGs. A. Volcano plot of IMRGs in TCGA-LUAD database. Green and red dots represent the genes that are significantly down-regulated and up-regulated, respectively. Black dots represent no differentially expressed genes; B, C. LASSO Cox regression was performed to identify the differentially expressed IMRGs closely related to the prognosis of LUAD; D. Multivariate cox analysis to develop a prognostic index based on these IMRGs. LASSO, least absolute shrinkage and selection operator.

was enrichment in the lipid oxidation, complement activation, transcytosis, regulation of lipopolysaccharide mediated signaling pathway, and regulation of fatty acid oxidation (**Figure 7A**; Table S3). KEGG analysis indicated that the HR group was enriched in the cell cycle, pyrimidine metabolism, oocyte meiosis, nucleotide excision repair, and proteasome. The LR group was enriched in the fatty acid metabolism, PPAR signaling pathway, glycosphingolipid metabolism, histidine and tryptophan metabolism (**Figure 7B**; Table S3).

Immune infiltration analysis and immunotherapy response prediction

ESTIMATE algorithm suggested the LR group had significantly higher stromal, immune, and ESTIMATE scores and lower tumor purity than the HR group (**Figure 8A-D**).The risk score was negatively correlated with the stromal, immune, and ESTIMATE scores and positively correlated with tumor purity (**Figure 8E-H**). Single-sample Gene Set Enrichment Analysis (ssGSEA) was used to compare immune-related gene-set

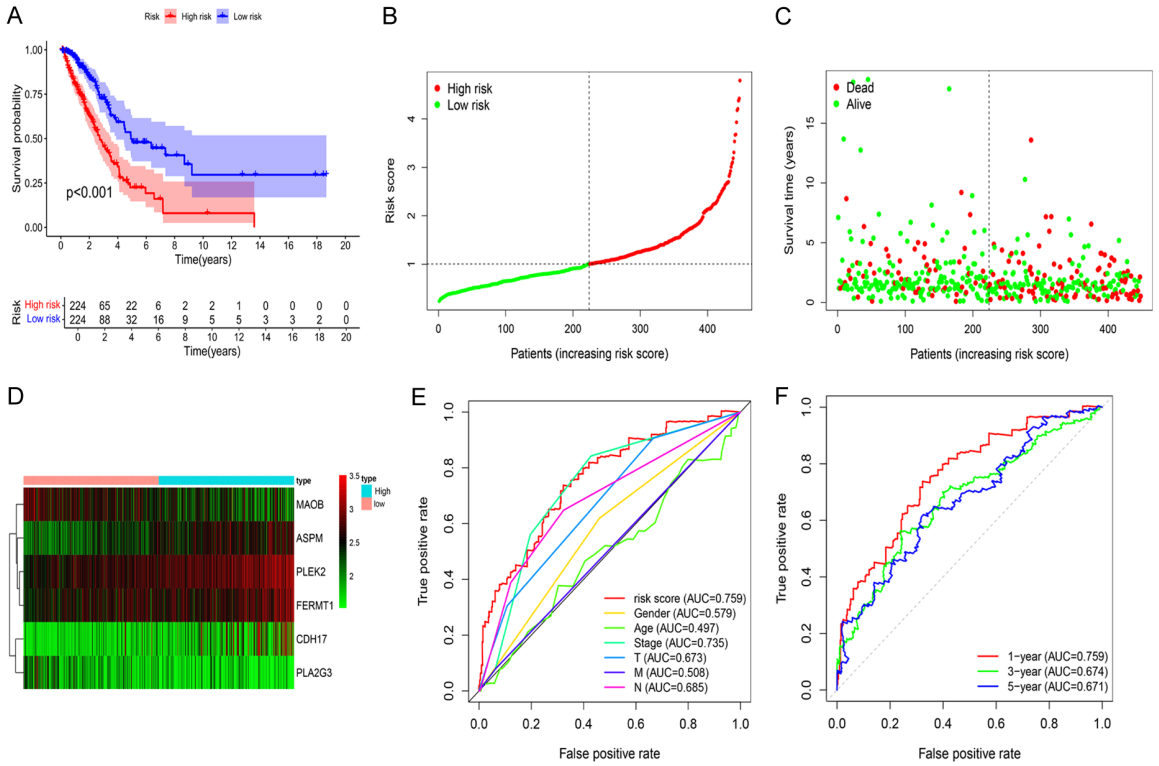


Figure 3. Validation of the predictive performance of IMRGs signature. (A) Kaplan-Meier survival curves of OS between LR and HR groups in the training cohort; (B-D) Risk scores (B), survival outcome (C) and the model genes (D) between LR and HR groups in the training cohort; (E) Comparing the AUCs of the risk scores with other clinical parameters in the training cohort; (F) Time-dependent ROC analysis of risk scores for predicting the OS in the training cohort. OS, overall survival; LR, low-risk; HR, high-risk; AUC, area under the curve.

enrichment scores between the two groups. The HR group showed higher enrichment scores for inflammation-promoting features, Natural killer (NK) cells and Major Histocompatibility Complex class I (MHC-I). In contrast, the LR group showed higher enrichment scores for activated dendritic cells (aDCs), B cells, dendritic cells (DCs), immature dendritic cells (iDCs), mast cells, neutrophils, plasmacytoid dendritic cells (pDCs), T-helper cells, tumor-infiltrating lymphocytes (TILs), Human Leukocyte Antigen (HLA) and type II interferon response (Type-II-IFN)-Response (**Figure 8I**, **8J**).

To further investigate the potential association between the IMRGs prognostic signature and response to immunotherapy, we compared the expression of immune checkpoint genes between the two risk groups. Six immune checkpoints were up-regulated in the HR group, including TNFRSF9 (4-1BB), CD276, TNFSF4, CD274 (PD-L1), TNFSF9, and TNFRSF18, whereas CD40LG, VSIR, SELPLG, CD48, CD160, TNFSF18, TNFSF14, ADORA2A, CD27, TNFRSF14, CD200R1, LGALS9, CD28, TNFSF15, BTLA, and IDO2 were up-regulated in the LR group (**Figure 9A**). IPS was used to assess the therapeutic efficacy of ICBs, our results indicated that the LR group had higher IPS scores (**Figure 9B-E**). The TIDE algorithm showed that patients in the HR group have higher TIDE scores, suggesting a higher likelihood of immune escape and a poorer predicted response to immunotherapy in this group (**Figure 9F**). Consistent with these findings, TIDE predicted a higher proportion of responders to immunotherapy in the LR group than in the HR group (**Figure 9G**). TMB, a validated predictive biomarker for ICB response across various cancer types [32], was significantly higher in the HR cohort and positively correlated with the risk score ($R = 0.3$, $P < 0.001$; **Figure 9H**, **9I**). The HR group also showed a significantly higher frequency of somatic mutations than the LR group (**Figure 9J**, **9K**). Moreover, TP53 and TTN, the most frequently mutated genes, showed a significantly higher mutation frequency in the HR group than in the LR group

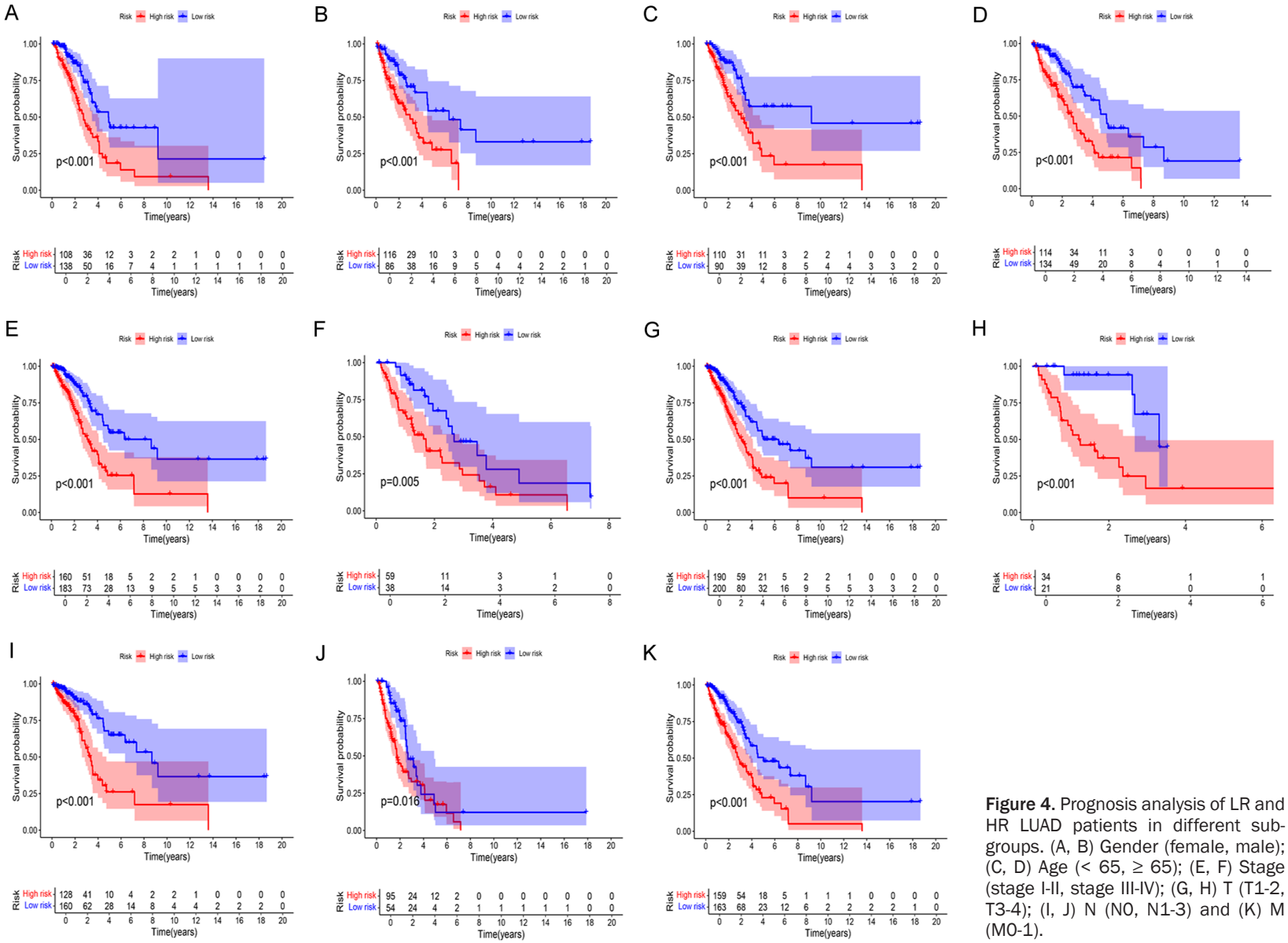


Figure 4. Prognosis analysis of LR and HR LUAD patients in different subgroups. (A, B) Gender (female, male); (C, D) Age (< 65, ≥ 65); (E, F) Stage (stage I-II, stage III-IV); (G, H) T (T1-2, T3-4); (I, J) N (N0, N1-3) and (K) M (M0-1).

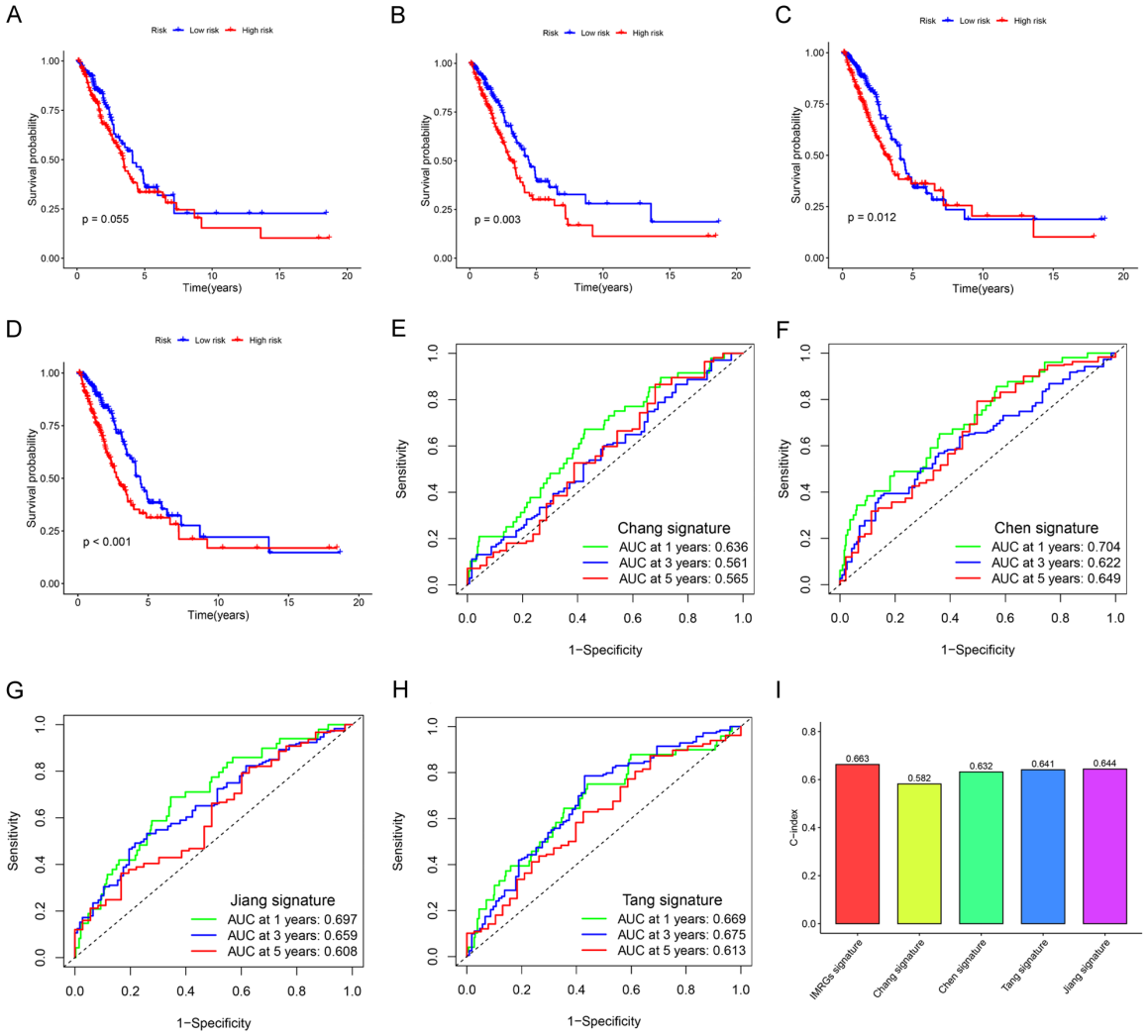


Figure 5. Comparison of the IMRGs prognostic signature with the published signatures. The Kaplan-Meier survival curve and ROC curve of the three-gene signature developed by Chang *et al.* (Chang signature; A, E), the sixteen-gene signature established by Chen *et al.* (Chen signature; B, F), the six-gene signature created by Jiang *et al.* (Jiang signature; C, G), and the four-gene signature established by Tang *et al.* (Tang signature; D, H); (I) A comparison of the C-indexes for the five prognostic models. All published signatures were recalculated using the same Z score standardized expression matrix as our model to ensure a fair comparison.

(**Figure 9J**, **9K**). These analyses are based on computational predictions and warrant experimental validation.

Tumor stemness analysis

Stemness-related biomarkers in tumor cells have been associated with drug resistance, cancer recurrence, and proliferation [33]. The levels of both RNAss and DNAss were significantly higher in the HR group than in the LR group (**Figure 10A**, **10B**). Spearman correlation analysis showed a positive correlation between the risk score and these two stemness indices (**Figure 10C**, **10D**). These observations suggest more active tumor-initiating cells in the HR group.

Chemotherapy response prediction

To explore the potential clinical significance of the IMRGs prognostic signature in guiding therapeutic strategies for LUAD patients, we used the "pRRophetic" algorithm to estimate the IC_{50} values of several chemotherapeutic agents and compared them between the LR and HR groups. IC_{50} values are inversely correlated with drug sensitivity, with lower values indicating greater predicted drug efficacy. The LR group showed significantly higher IC_{50} values than the

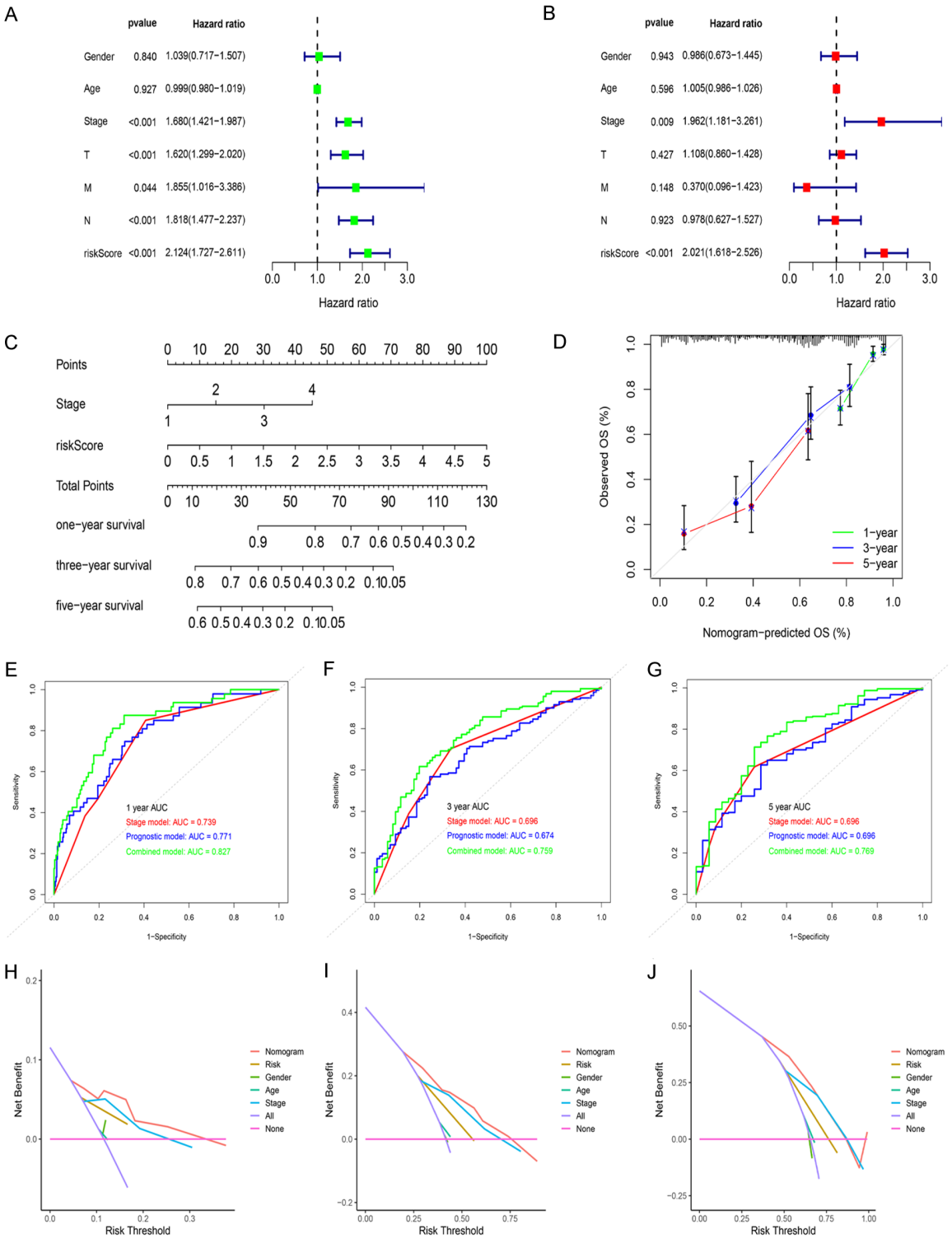


Figure 6. Construction of the nomogram based on the IMRGs signature and clinical stage. (A) Univariate and (B) multivariate Cox regression analysis based on the IMRGs risk score and clinical variables; (C) The nomogram for predicting the OS at 1, 3, and 5 years; (D) Calibration curve for consistency between 1-, 3-, or 5-year nomogram predicted survival and actual survival; (E-G) ROC curves of 1-, 3-, and 5-year OS based on the stage, IMRGs signature, and the nomogram; (H-J) The DCA curves used for predicting the OS at 1-, 3-, and 5-year. DCA, Decision curve analysis.

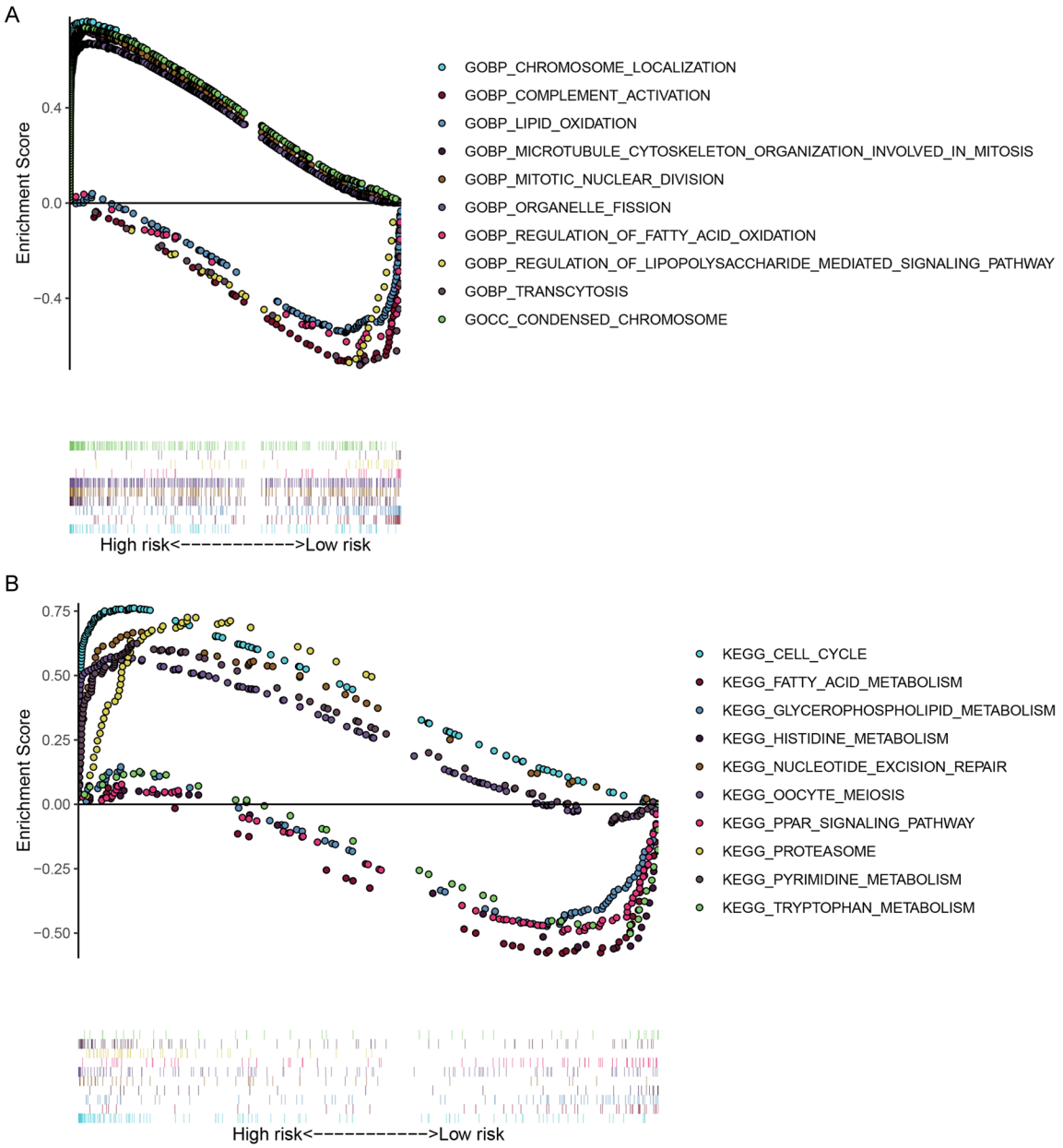


Figure 7. The functional enrichment analysis based on the IMRGs signature. A. GO enrichment analysis; B. KEGG enrichment analysis. GO, Gene Ontology; KEGG, Kyoto Encyclopedia of Genes and Genomes.

HR group for cisplatin, paclitaxel, docetaxel, etoposide, gemcitabine, mitomycin C, and vinblastine (**Figure 11A-G**), suggesting that HR patients may have enhanced chemotherapeutic responsiveness, although this requires clinical validation.

Functional analysis and in vitro experiments of the prognostic gene CDH17 in LUAD

CDH17 has recently been examined as a biomarker for diagnostic and prognostic stratification across several malignancies [34-39], and CDH17 knockdown has been reported to suppress hepatocellular carcinoma cell proliferation and promote apoptosis *in vitro* [40]. To elucidate its potential roles in LUAD, we used enrichment analyses and found that it was linked to multiple oncogenic and immunomodulatory pathways, including TNF-JNK/TNF-p38 inflammatory signaling, JAK-STAT cytokine signaling, protein activation cascade, estrogen metabolic process, and extrinsic and intrinsic

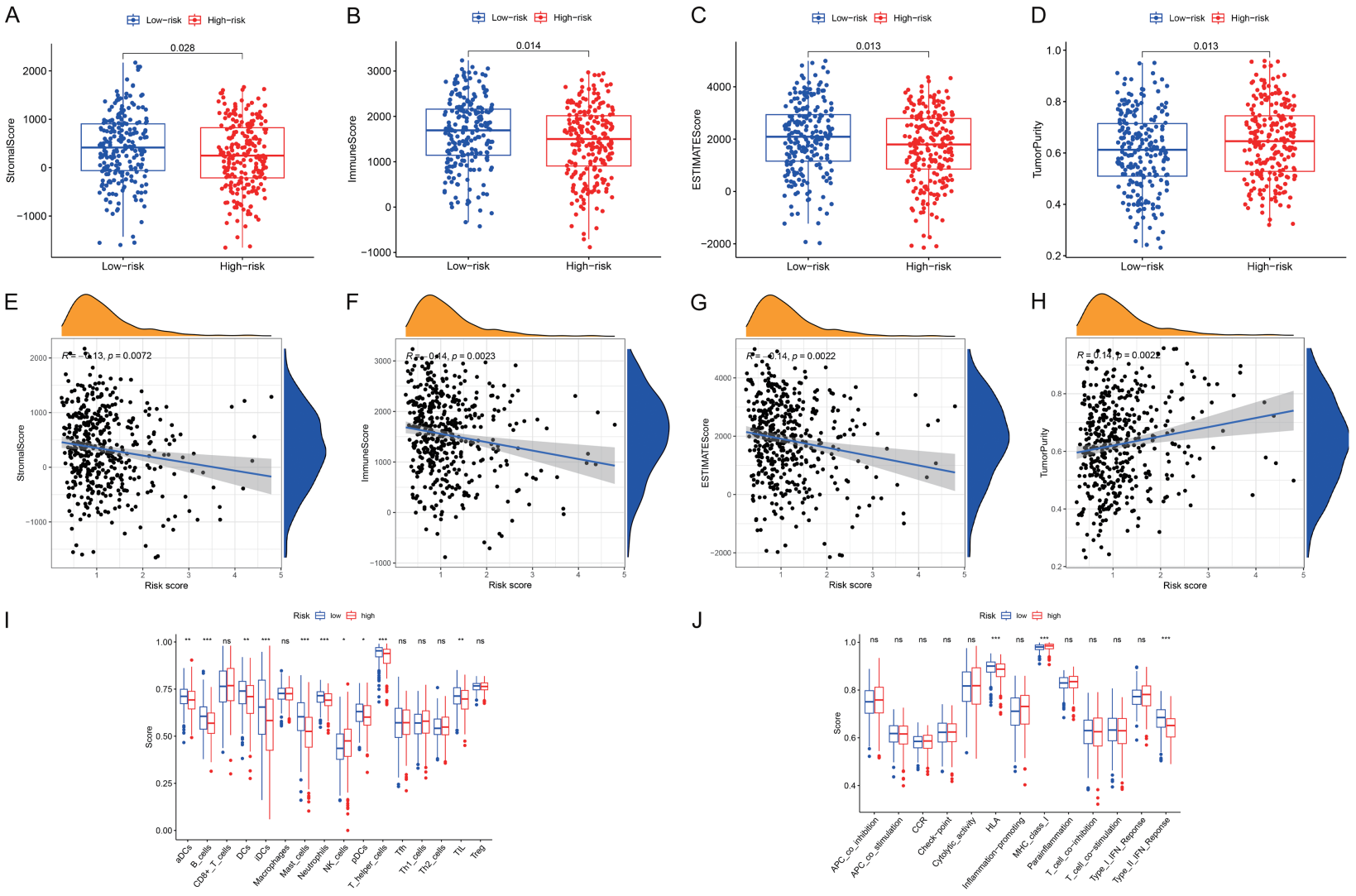


Figure 8. The difference observed between the LR and HR groups in the immune microenvironment. A-D. Differences in stromal score, immune score, estimated score, and tumor purity between the LR and HR populations; E-H. Correlation between the stromal score, immune score, estimated score and tumor purity with the risk score; I. ssGSEA analysis of differences in 16 types of immune cell infiltration in the TME between the LR and HR groups; J. The correlation between the prognostic signature and the 13 immune-related functions. *P* value < 0.05 indicates statistical significance. *, *P* < 0.05; **, *P* < 0.01; ***, *P* < 0.001; ns, non-significant. ssGSEA, Single-sample Gene Set Enrichment Analysis; TME, tumor microenvironment.

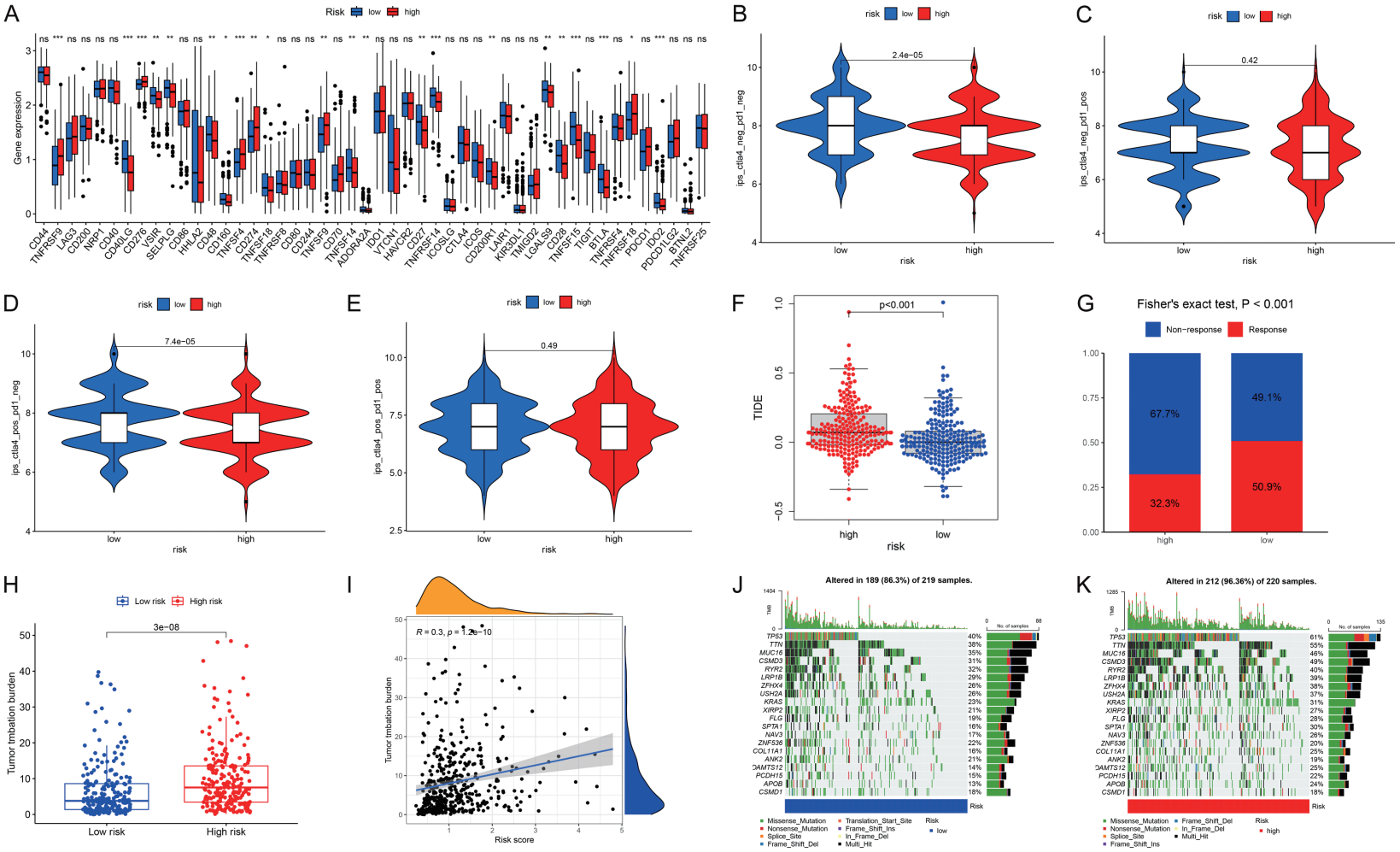


Figure 9. The prediction of immunotherapeutic response based on IMRGs prognostic signature. A. The expression of 48 immune checkpoints differs between the LR and HR groups. The red boxes represent HR patients, while the blue boxes represent LR patients; B-E. Differential analysis of IPS between the LR and HR populations; F. Differential analysis of TIDE scores between the LR and HR populations; G. Distribution of immunotherapy beneficiaries between the LR and HR groups; H. The difference of TMB between the LR and HR groups; I. Association between TMB and risk scores; J, K. The differences in TMB in somatic cells in patients with LUAD between the LR and HR groups; *P* value < 0.05 indicates statistical significance. *, *P* < 0.05; **, *P* < 0.01; ***, *P* < 0.001. IPS, Immunophenoscore; TIDE, tumor Immune Dysfunction and Exclusion; TMB, tumor mutational burden.

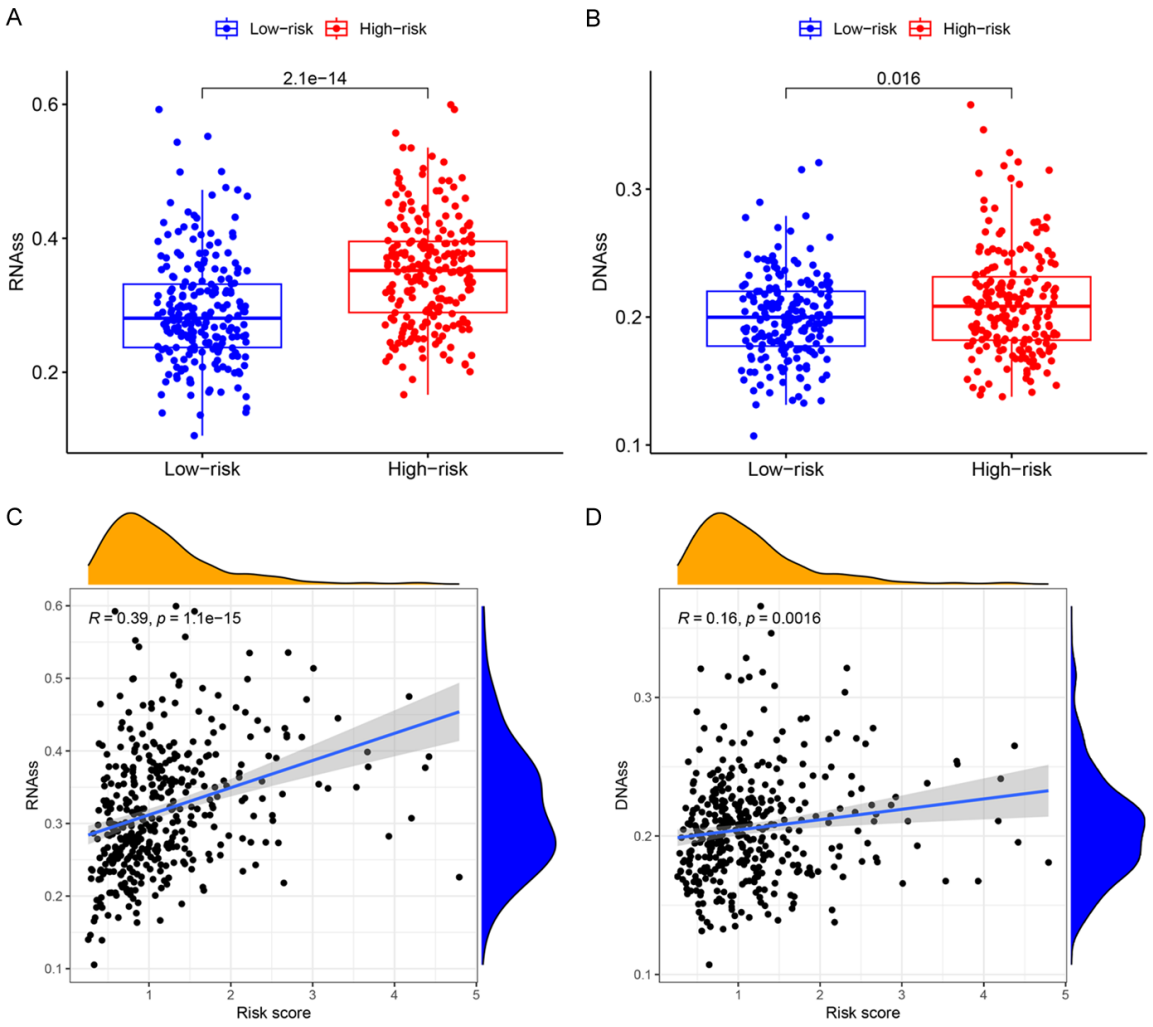


Figure 10. Comparison of RNA and DNA stemness scores between the HR and LR subgroups. A, B. Differences in RNAss and DNAss between the LR and HR populations; C, D. The relationship between risk score and both RNAss or DNAss. RNAss, RNA stemness score; DNAss, DNA stemness score.

apoptotic crosstalk. These pathways have been associated with tumorigenesis, aberrant proliferation, apoptosis resistance, and immunosuppression (**Figure 12A**, **12B**). Consistently, TCGA transcriptomic data, immunohistochemical staining, and Kaplan-Meier survival analysis suggested that CDH17 was upregulated in LUAD tissues and that higher expression was associated with a poorer prognosis (**Figure 12C-F**).

To assess its biological role, we compared CDH17 expression between normal bronchial epithelial BEAS-2B cells and LUAD cell lines (A549 and H1299). CDH17 mRNA was higher in H1299 than in BEAS-2B cells (**Figure 13A**), and Western blotting showed higher CDH17 protein in both A549 and H1299 cells relative to BEAS-2B cells (**Figure 13B**). Because H1299 cells displayed relatively high baseline CDH17 expression, we used this line for siRNA-mediated knockdown. Three CDH17-targeting siRNAs were transfected into H1299 cells, and knockdown efficiency was confirmed by RT-qPCR and Western blot. Among them, only si-CDH17-935 reduced CDH17 mRNA and protein to levels clearly below those in the siRNA-negative control (si-NC) cells (**Figure 13C**, **13D**). This siRNA was therefore used in all subsequent experiments. Silencing CDH17 with si-CDH17-935 lowered the viability of H1299 cells at 24, 48, and 72 h in the CCK-8 assay (**Figure 13E**), and reduced colony-forming capacity relative to si-NC cells (**Figure 13F**). To determine whether this effect involved apoptosis, we performed Annexin V-APC/PI double staining and quanti-

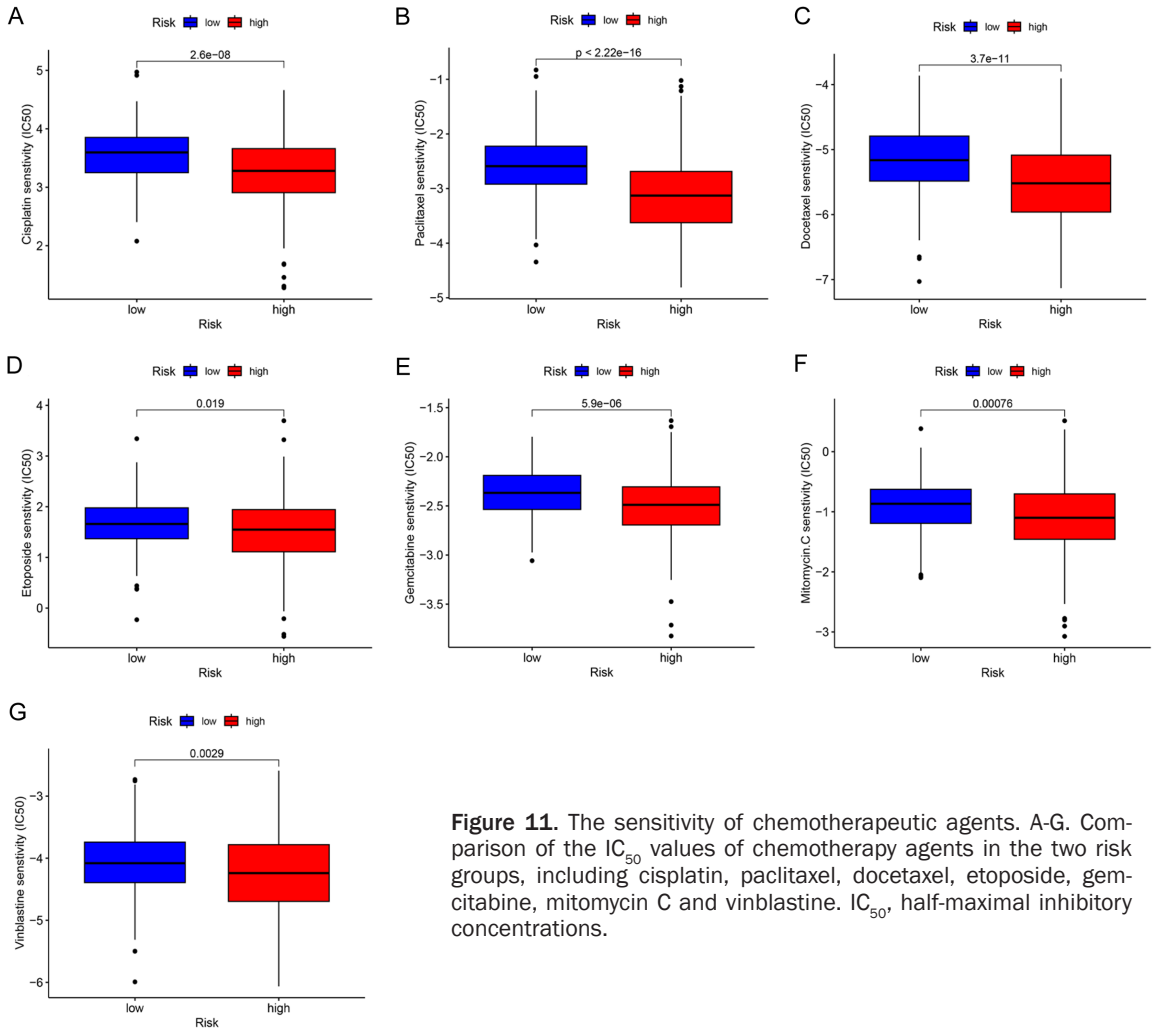


Figure 11. The sensitivity of chemotherapeutic agents. A-G. Comparison of the IC_{50} values of chemotherapy agents in the two risk groups, including cisplatin, paclitaxel, docetaxel, etoposide, gemcitabine, mitomycin C and vinblastine. IC_{50}, half-maximal inhibitory concentrations.

fied apoptotic cells by flow cytometry. The proportion of apoptotic cells was higher in the si-CDH17-935 group than in the si-NC group (**Figure 13G**), suggesting that CDH17 knockdown enhances apoptosis in H1299 cells.

Discussion

The emergence of immunotherapy has improved clinical outcomes in LUAD. However, considerable interpatient heterogeneity in immunotherapy efficacy persists, which has been partly attributed to variations in TME characteristics [41, 42]. Immune cell infiltration and metabolic reprogramming within the TME have both been linked to immunotherapy outcomes in LUAD [8, 9, 43, 44], and metabolism and antitumor immunity are closely interconnected [12, 13]. Furthermore, immune-associated genes or metabolism-associated genes have been implicated in LUAD, and several prognostic biomarkers based on these genes have been developed for prognostic and therapeutic guidance [31, 45, 46]. Combined predictors reflecting both immune and metabolic status have also shown promise as prognostic signatures [14, 15]. Based on the above observations, we performed gene screening by intersection analysis and developed an IMRG-based prognostic signature for LUAD, which was further validated in internal as well as external patient cohorts.

In our present study, we stratified patients with LUAD into LR and HR groups based on the median risk score calculated from the IMRG-based signature. Kaplan-Meier survival analysis showed poorer OS for the HR group. Higher risk scores were additionally associated with advanced clinical stage, T stage, and N stage, supporting the potential prognostic value of

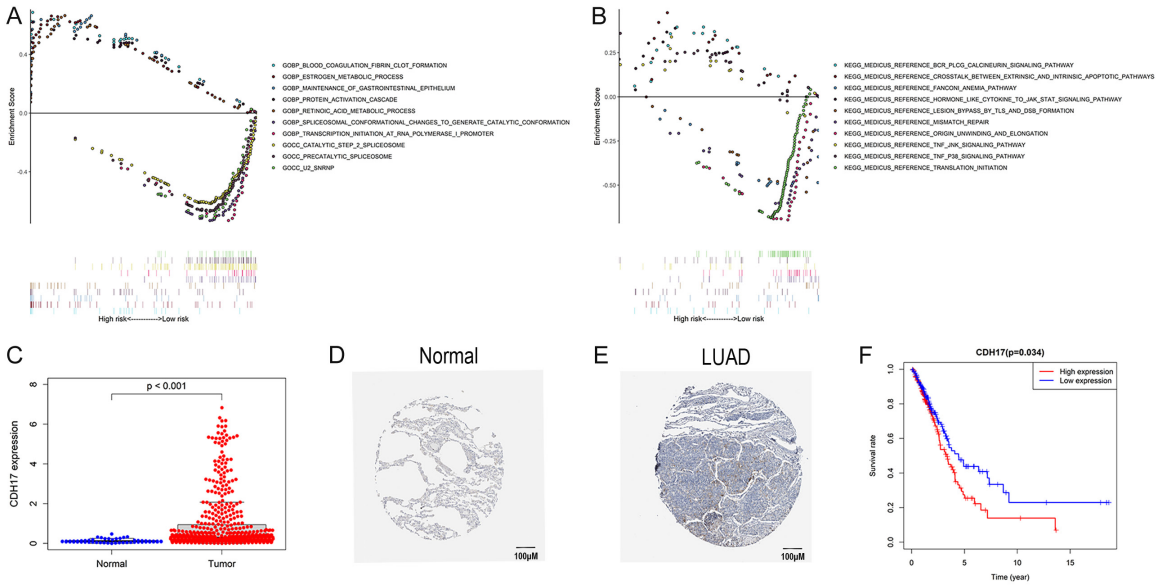


Figure 12. The functional enrichment analysis of CDH17. A. GO enrichment analysis. B. KEGG enrichment analysis. C. Data from the TCGA database indicating that CDH17 is more highly expressed in LUAD tissues than in normal tissues. D, E. Immunohistochemical staining images were obtained from the Human Protein Atlas (HPA, https://www.proteinatlas.org/ENSG00000079112-CDH17/tissue/lung#img and https://www.proteinatlas.org/ENSG00000079112-CDH17/cancer/lung+cancer#img), showing CDH17 expression in human normal lung tissue and LUAD tissue. The magnification is 40× Scale bar, 100 μm. F. Kaplan-Meier survival curves of patients with high versus low expression of CDH17 in the TCGA database.

this signature. ROC curve and C-index analyses further indicated that our signature achieved competitive predictive efficacy compared with four previously published LUAD prognostic signatures [28-31]. In addition to this quantitative advantage, our model is distinct from other recent immune- or metabolism-based signatures [31, 45-48] in that it uniquely intersects both immune- and metabolism-related genes and incorporates CDH17 as a novel experimentally validated component. To explore the clinical translational potential of this signature, we developed a nomogram integrating the risk score and clinical characteristics to enable individualized survival prediction for LUAD patients.

To explore potential immune-related mechanisms underlying the prognostic performance of the signature in LUAD, we performed the ssGSEA algorithm to compare immune infiltration status and immune functional scores between the LR and HR groups. Our results indicated that the LR group may obtain greater immunotherapeutic benefits. Specifically, the LR cohort presented elevated enrichment scores of mast cells, DCs and TILs, and these higher enrichment levels have previously been associated with better clinical outcomes in lung cancer [49-51]. In addition, the LR group showed higher HLA-related gene-set scores and lower MHC-I-associated gene-set scores. Functionally, this may partly explain why this group tends to respond better to immunotherapy. Previous studies have shown that HLA molecules are important for neoantigen presentation, and loss of HLA-mediated antigen presentation can facilitate tumor immune escape [52, 53]. Higher MHC-I-associated gene-set scores in the HR group may facilitate immune escape, whereby the MHC-I subunit β2-microglobulin interacts with the inhibitory receptor LILRB1 on macrophages, thereby protecting tumor cells from phagocytosis and conferring immunotherapy resistance [54].

Recent studies have shown that ICBs therapy yields meaningful clinical benefits in cancer patients [55-58]. In this study, we explored whether our IMRGs prognostic signature could help predict responses to ICBs treatment in LUAD. We analyzed the associations between the risk score and the expression of immune checkpoint genes, IPS, TIDE, as well as TMB. These results were consistent with our previous

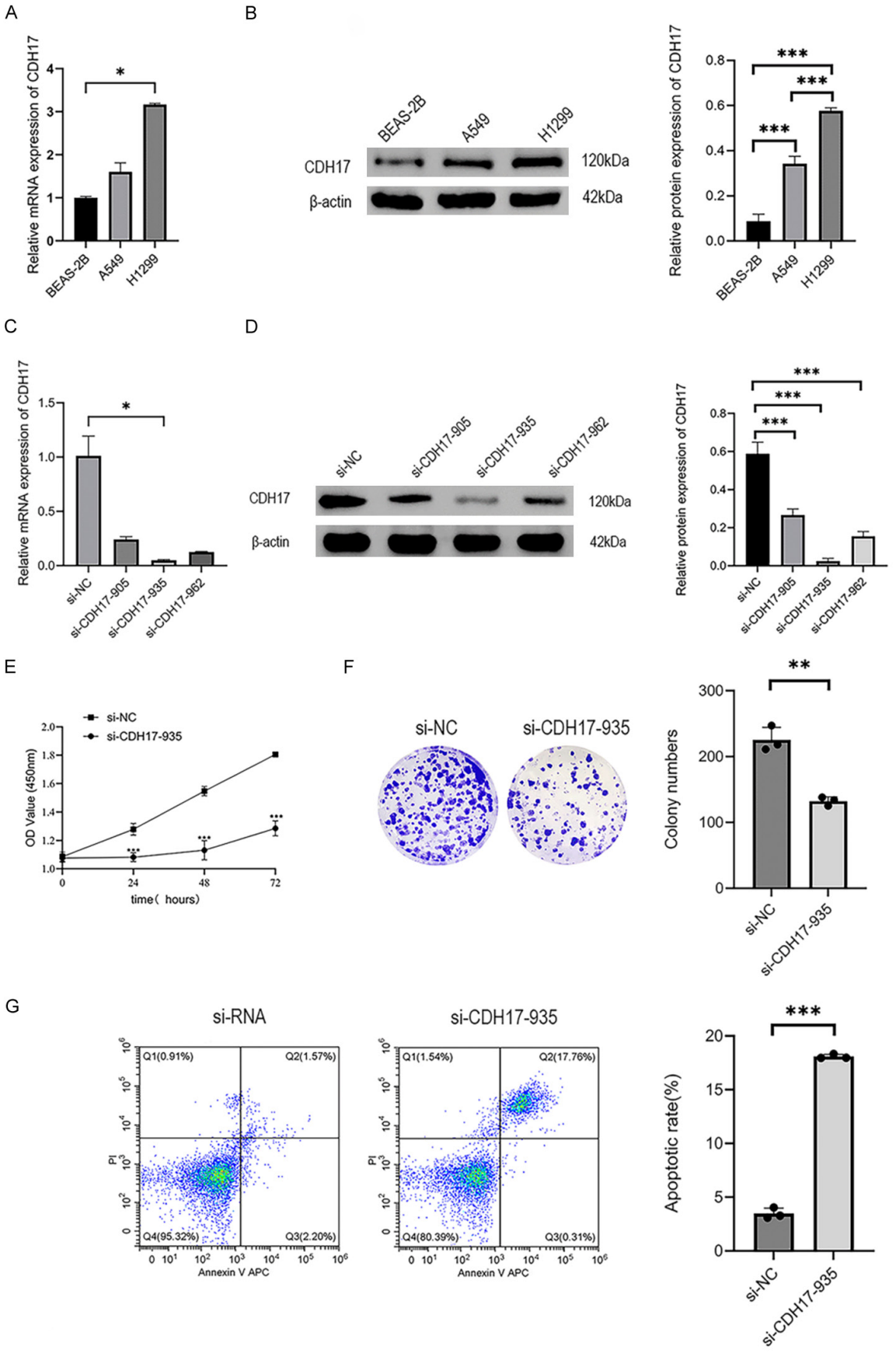

A
Relative mRNA expression of CDH17
BEAS-2B
A549
H1299
B
CDH17
β-actin
120kDa
42kDa
Relative protein expression of CDH17
C
si-NC
si-CDH17-905
si-CDH17-935
si-CDH17-962
D
E
OD Value (450nm)
time(hours)
F
Colony numbers
G
si-RNA
si-CDH17-935
Q1(0.91%)
Q2(1.57%)
Q4(95.32%)
Q3(2.20%)
Q1(1.54%)
Q2(17.76%)
Q4(80.39%)
Q3(0.31%)
PI
Annexin V APC
Apoptotic rate(%)

Figure 13. Experimental validation of key prognostic gene CDH17 in the 6-IMRG signature: impact on LUAD cell proliferation and apoptosis. A, B. RT-qPCR and Western blot verified the expression level of CDH17 in normal bronchial epithelial BEAS-2B cells and LUAD cell lines. C, D. RT-qPCR and Western blot verified CDH17 expression levels after siRNA-mediated silencing in H1299 cells. E. The proliferation of cells in CDH17-silenced and si-NC groups at 24, 48, and 72 h were detected by CCK-8 method in H1299 cells. F. Colony formation in CDH17-silenced and si-NC groups in H1299 cells. G. Distribution of apoptosis in CDH17-silenced and si-NC groups in H1299 cells. si-NC, small interfering RNA-negative control; CCK-8, Cell Counting Kit-8.

ssGSEA findings. Higher PD-L1 expression within the HR group may facilitate tumor mediated immunosuppression via binding to PD-1 on T cell surfaces [59], and this phenomenon has been linked to unfavorable outcomes in several solid tumors including LUAD [60]. Of note, the HR group also showed increased transcript levels for the co-stimulatory molecules TNFRSF9 (4-1BB) and TNFRSF18 (GITR). Based on the higher TIDE scores observed in the HR patients, the elevated expression of these two co-stimulatory genes might be interpreted as a compensatory exhaustion response [61, 62]. Consistent with this finding, IPS analysis further suggested that HR LUAD patients tended to have lower predicted ICBs responsiveness. Interestingly, the LR group had substantially lower TMB (an indicator of tumor immunogenicity), yet TIDE results predicted that more LR patients would respond to ICB therapy. This observation raises the possibility that tumor immune infiltration and immune functions could exert a stronger influence on immunotherapy outcomes than TMB based immunogenicity alone. These integrative analyses imply that the IMRGs prognostic signature may be associated with immunotherapy response. Still, these conclusions are derived purely from bioinformatic predictions and need further clinical validation.

Chemotherapy continues to play an essential role in the management of LUAD, administered either as monotherapy or combined with other regimens [63]. We furthermore explored the relationship between our IMRGs signature and chemotherapeutic responses. Drug sensitivity analyses suggested that the HR group might be more sensitive to microtubule-targeting drugs. This possibility was partially supported by GSEA, which revealed enrichment of cell cycle and oocyte meiosis pathways in this group. These pathways involve key regulators of mitosis and microtubule function. Their enrichment may reflect a hyperproliferative phenotype, which could partly explain why the HR group is predicted to be more sensitive to microtubule-targeting drugs such as docetaxel, paclitaxel, and vinblastine. We also assessed two tumor stemness indices, RNAss and DNAss, both of which are associated with tumor proliferation, invasion, metastasis, and chemoresistance [25]. The HR group showed significantly higher values for both indices than the LR group, which may partly explain the unfavorable prognosis of the HR group. Together, these analyses suggest that the HR group may be more proliferative and stemness-enriched. Nevertheless, these findings are exploratory, and further functional validation is needed prior to considering any clinical implications for chemotherapy.

The six IMRGs in our signature are ASPM, PLEK2, FERMT1, MAOB, PLA2G3, and CDH17. Five of these genes have previously been reported to be associated with LUAD. ASPM regulates the mitotic spindle and promotes LUAD cell proliferation, migration, invasion, and metastasis [64, 65]. PLEK2 is a pleckstrin family protein. Its knockdown in LUAD cells markedly suppressed proliferation and migration and increased apoptosis. Moreover, tumor growth in mice injected with PLEK2-silencing LUAD cells was impaired [66]. FERMT1 is upregulated in tumor tissue compared with normal tissue, and its depletion reduces LUAD cell migration and invasion [67]. MAOB is downregulated in LUAD tissues and cell lines. Its overexpression suppresses proliferation, migration, and invasion *in vitro* and tumor growth in mice [68]. PLA2G3 is a lipid metabolism-related secreted phospholipase A2 that appears in several LUAD prognostic signatures and is expressed at lower levels in LUAD cell lines than in BEAS-2B cells [69-71]. These findings support the biological plausibility of our signature and suggest that ASPM, PLEK2, and FERMT1 may contribute to the aggressive behavior of the HR group.

CDH17, the remaining IMRG in our signature, is relatively poorly characterized in LUAD. A member of the cadherin superfamily, it is widely overexpressed in digestive system malignan-

cies, including colorectal [72, 73], gastric [38, 74], cholangiocellular [36], hepatocellular [40, 75], and pancreatic cancers [76]. Its role as an oncogene has been well documented, and substantial clinical data suggest its potential utility as a diagnostic biomarker in these tumor types [77]. Its prognostic value has also been reported in gastric and colorectal cancers [35, 78]. Our bioinformatic analyses indicated that CDH17 is upregulated in LUAD, and that its upregulation is correlated with poor patient prognosis. Functional enrichment analysis of genes differentially expressed between CDH17-high and CDH17-low LUAD samples suggested that these genes were enriched in pathways related to oncogenesis and malignant progression, implying a potential involvement of CDH-17 in LUAD pathogenesis. Nevertheless, these observations derive solely from transcriptome-based enrichment results. Although transcriptomic analyses in LUAD have linked elevated CDH17 to signatures of immunosuppressive TME, direct experimental evidence demonstrating that CDH17 mediates immune regulation or metabolic reprogramming in LUAD cells is still lacking [79]. Therefore, its potential roles in these biological processes remain to be further validated. Consistent with a previous report [80], our findings also showed CDH17 upexpressed in LUAD cell lines. To further investigate its role in LUAD, we performed a series of *in vitro* assays. Our results showed that CDH17 silencing suppressed LUAD cell proliferation and increased apoptosis. Overall, our study provides preliminary evidence for a potential oncogenic role of CDH17 in LUAD and supports its potential as a therapeutic target, warranting further investigation.

Despite these promising findings, several limitations of our study should be acknowledge. First, both the IMRGs prognostic signature and the nomogram were derived from retrospective data. Thus, prospective validation in large, multicenter cohorts is essential. Second, additional *in vivo* animal experiments are warranted to corroborate the biological functions of CDH17 in LUAD progression. Third, we did not explore whether a CDH17 inducer could counteract its pro-tumor effects on LUAD cell proliferation and apoptosis regulation. Future work will focus on resolving these issues to deepen our understanding and address the remaining challenges. Fourth, although the signature was constructed from IMRGs, our analyses were primarily based on transcriptomic association, enrichment, and bioinformatics-based predictions and therefore do not provide direct mechanistic evidence of immune-metabolic crosstalk. The *in vitro* assessment of CDH17 was limited to proliferation, colony formation, and apoptosis, and no metabolic and immune-related phenotypes were assessed. In addition, colony formation was assessed after transient CDH17 knockdown. Given that transient silencing lasts only a few days while the assay takes 14 days, this result should be interpreted with caution, as reflecting the effect of early CDH17 knockdown rather than sustained knockdown. Future studies should include metabolic flux analysis, glucose/lactate measurements, immune co-culture, and *in vivo* models, as well as stable knockdown or knockout systems, to investigate the mechanistic role of CDH17 in LUAD.

Conclusions

We developed and validated an IMRG-based prognostic signature for LUAD.

Bioinformatics analyses suggested that the signature may be associated with immunotherapy response and chemotherapy response. However, these findings are exploratory and require experimental validation. *In vitro* assays suggested that CDH17 may promote proliferation and reduce apoptosis in LUAD cells.

Acknowledgements

This research was supported by the Natural Science Foundation of Hunan Province, grant number 2024JJ8228.

Disclosure of conflict of interest

None.

Address correspondence to: Shao Liu, Department of Pharmacy, Xiangya Hospital, Central South University, No. 87 Xiangya Road, Kaifu District, Changsha 410008, Hunan, China. E-mail: liushao999@csu.edu.cn; Lan Fan, Department of Clinical Pharmacology, Xiangya Hospital, Central South University, No. 110 Xiangya Road, Kaifu District, Changsha 410078, Hunan, China. E-mail: fanlanxyyy@163.com

References

[1] Siegel RL, Giaquinto AN and Jemal A. Cancer statistics, 2024. CA Cancer J Clin 2024; 74: 12-49.

[2] Herbst RS, Morgensztern D and Boshoff C. The biology and management of non-small cell lung cancer. Nature 2018; 553: 446-454.

[3] Duma N, Santana-Davila R and Molina JR. Non-small cell lung cancer: epidemiology, screening, diagnosis, and treatment. Mayo Clin Proc 2019; 94: 1623-1640.

[4] Gao L, Xia L, Ji W, Zhang Y, Xia W and Lu S. Knockdown of CDK5 down-regulates PD-L1 via the ubiquitination-proteasome pathway and improves antitumor immunity in lung adenocarcinoma. Transl Oncol 2021; 14: 101148.

[5] Shan Q, Zhang Y and Liang Z. Clustering analysis and prognostic signature of lung adenocarcinoma based on the tumor microenvironment. Sci Rep 2022; 12: 12059.

[6] Shang S, Wang MZ, Xing Z, He N and Li S. Lactate regulators contribute to tumor microenvironment and predict prognosis in lung adenocarcinoma. Front Immunol 2022; 13: 1024925.

[7] Hanahan D and Weinberg RA. Hallmarks of cancer: the next generation. Cell 2011; 144: 646-74.

[8] Petitprez F, Vano YA, Becht E, Giraldo NA, de Reyniès A, Sautès-Fridman C and Fridman WH. Transcriptomic analysis of the tumor microenvironment to guide prognosis and immunotherapies. Cancer Immunol Immunother 2018; 67: 981-988.

[9] Qiu L, Yang Z, Jia G, Liang Y, Du S, Zhang J, Liu M, Zhao X and Jiao S. Clinical significance and immune landscape of a novel immune cell infiltration-based prognostic model in lung adenocarcinoma. Heliyon 2024; 10: e33109.

[10] Cai W, Zhou D, Wu W, Tan WL, Wang J, Zhou C and Lou Y. MHC class II restricted neoantigen peptides predicted by clonal mutation analysis in lung adenocarcinoma patients: implications on prognostic immunological biomarker and vaccine design. BMC Genomics 2018; 19: 582.

[11] Zaric B, Brcic L, Buder A, Brandstetter A, Buresch JO, Traint S, Kovacevic T, Stojsic V, Perin B, Pirker R and Filipits M. PD-1 and PD-L1 protein expression predict survival in completely resected lung adenocarcinoma. Clin Lung Cancer 2018; 19: e957-e963.

[12] Yang L, Chu Z, Liu M, Zou Q, Li J, Liu Q, Wang Y, Wang T, Xiang J and Wang B. Amino acid metabolism in immune cells: essential regulators of the effector functions, and promising opportunities to enhance cancer immunotherapy. J Hematol Oncol 2023; 16: 59.

[13] Huang Q, Fan L, Gong M, Ren J, Chen C and Xie S. Metabolic reprogramming in lung cancer and its clinical implication. Front Pharmacol 2024; 15: 1516650.

[14] Guo Y, Yang J, Gao H, Tian X, Zhang X and Kan Q. Development and verification of a combined immune- and metabolism-related prognostic signature for hepatocellular carcinoma. Front Immunol 2022; 13: 927635.

[15] Xiao Y, Zhang G, Wang L and Liang M. Exploration and validation of a combined immune and metabolism gene signature for prognosis prediction of colorectal cancer. Front Endocrinol (Lausanne) 2022; 13: 1069528.

[16] Bhattacharya S, Andorf S, Gomes L, Dunn P, Schaefer H, Pontius J, Berger P, Desborough V, Smith T, Campbell J, Thomson E, Monteiro R, Guimaraes P, Walters B, Wiser J and Butte AJ. ImmPort: disseminating data to the public for the future of immunology. Immunol Res 2014; 58: 234-239.

[17] Liberzon A, Birger C, Thorvaldsdóttir H, Ghandi M, Mesirov JP and Tamayo P. The molecular signatures database (MSigDB) hallmark gene set collection. Cell Syst 2015; 1: 417-425.

[18] Ritchie ME, Phipson B, Wu D, Hu Y, Law CW, Shi W and Smyth GK. limma powers differential expression analyses for RNA-sequencing and microarray studies. Nucleic Acids Research 2015; 43: e47.

[19] Friedman JH, Hastie T and Tibshirani R. Regularization paths for generalized linear models via coordinate descent. J Stat Softw 2010; 33: 1-22.

[20] Hänzelmann S, Castelo R and Guinney J. GSVA: gene set variation analysis for microarray and RNA-Seq data. BMC Bioinformatics 2013; 14: 7.

[21] Yoshihara K, Shahmoradgoli M, Martínez E, Vegesna R, Kim H, Torres-Garcia W, Treviño V, Shen H, Laird PW, Levine DA, Carter SL, Getz G, Stemke-Hale K, Mills GB and Verhaak RG. Inferring tumour purity and stromal and immune cell admixture from expression data. Nat Commun 2013; 4: 2612.

[22] Subramanian A, Tamayo P, Mootha VK, Mukherjee S, Ebert BL, Gillette MA, Paulovich A, Pomeroy SL, Golub TR, Lander ES and Mesirov JP. Gene set enrichment analysis: a knowledge-based approach for interpreting genome-wide expression profiles. Proc Natl Acad Sci U S A 2005; 102: 15545-15550.

[23] Jiang P, Gu S, Pan D, Fu J, Sahu A, Hu X, Li Z, Traugh N, Bu X, Li B, Liu J, Freeman GJ, Brown MA, Wucherpfennig KW and Liu XS. Signatures of T cell dysfunction and exclusion predict cancer immunotherapy response. Nat Med 2018; 24: 1550-1558.

[24] Charoentong P, Finotello F, Angelova M, Mayer C, Efremova M, Rieder D, Hackl H and Trajanoski Z. Pan-cancer immunogenomic analyses reveal genotype-immunophenotype relationships and predictors of response to checkpoint blockade. Cell Rep 2017; 18: 248-262.

[25] Malta TM, Sokolov A, Gentles AJ, Burzykowski T, Poisson L, Weinstein JN, Kamińska B, Huelsken J, Omberg L, Gevaert O, Colaprico A, Czerwińska P, Mazurek S, Mishra L, Heyn H, Krasnitz A, Godwin AK, Lazar AJ; Cancer Genome Atlas Research Network, Stuart JM, Hoadley KA, Laird PW, Noushmehr H and Wiznerowicz M. Machine learning identifies stemness features associated with oncogenic dedifferentiation. Cell 2018; 173: 338-354, e15.

[26] Geeleher P, Cox NJ and Huang RS. Clinical drug response can be predicted using baseline gene expression levels and in vitro drug sensitivity in cell lines. Genome Biol 2014; 15: R47.

[27] Yang W, Soares J, Greninger P, Edelman EJ, Lightfoot H, Forbes S, Bindal N, Beare D, Smith JA, Thompson IR, Ramaswamy S, Futreal PA, Haber DA, Stratton MR, Benes C, McDermott U and Garnett MJ. Genomics of Drug Sensitivity in Cancer (GDSC): a resource for therapeutic biomarker discovery in cancer cells. Nucleic Acids Res 2013; 41: D955-D961.

[28] Chang W, Li H, Zhong L, Zhu T, Chang Z, Ou W and Wang S. Development of a copper metabolism-related gene signature in lung adenocarcinoma. Front Immunol 2022; 13: 1040668.

[29] Chen M, Wang X, Wang W, Gui X and Li Z. Immune- and stemness-related genes revealed by comprehensive analysis and validation for cancer immunity and prognosis and its nomogram in lung adenocarcinoma. Front Immunol 2022; 13: 829057.

[30] Jiang Z, Luo Y, Zhang L, Li H, Pan C, Yang H, Cheng T and Chen J. A novel risk score model of lactate metabolism for predicting over survival and immune signature in lung adenocarcinoma. Cancers (Basel) 2022; 14: 3727.

[31] Tang B, Hu L, Jiang T, Li Y, Xu H, Zhou H, Lan M, Xu K, Yin J, Su C, Zhou C and Xu C. A metabolism-related gene prognostic index for prediction of response to immunotherapy in lung adenocarcinoma. Int J Mol Sci 2022; 23: 12143.

[32] Chan TA, Yarchoan M, Jaffee E, Swanton C, Quezada SA, Stenzinger A and Peters S. Development of tumor mutation burden as an immunotherapy biomarker: utility for the oncology clinic. Ann Oncol 2019; 30: 44-56.

[33] Luo Q and Vögeli TA. A methylation-based reclassification of bladder cancer based on immune cell genes. Cancers (Basel) 2020; 12: 3054.

[34] Ratto C, Sofo L, Ippoliti M, Merico M, Doglietto GB and Crucitti F. Prognostic factors in colorectal cancer. Literature review for clinical application. Dis Colon Rectum 1998; 41: 1033-1049.

[35] Ng L, Yu WS, Aung NM, Leung P, Luk JM, Wong DA, Sun S and Foo DC. Tissue cadherin 17 (CDH17): an important prognostic determinant of colorectal cancer using digital image analysis. Cancer Rep (Hoboken) 2024; 7: e70069.

[36] Zheng BH, Shen S, Wong KF, Gong ZJ, Sun WT, Ni XJ, Wang JW, Hu MY, Liu H, Ni XL, Liu HB, Luk JM and Suo T. Clinical correlation of cadherin-17 marker with advanced tumor stages and poor prognosis of cholangiocarcinoma. J Surg Oncol 2021; 123: 1253-1262.

[37] Wong BW, Luk JM, Ng IO, Hu MY, Liu KD and Fan ST. Identification of liver-intestine cadherin in hepatocellular carcinoma--a potential disease marker. Biochem Biophys Res Commun 2003; 311: 618-624.

[38] Altree-Tacha D, Tyrrell J and Haas T. CDH17 is a more sensitive marker for gastric adenocarcinoma than CK20 and CDX2. Arch Pathol Lab Med 2017; 141: 144-150.

[39] Park SS, Kang SH, Park JM, Kim JH, Oh SC, Lee JH, Chae YS, Kim SJ, Kim CS and Mok YJ. Expression of liver-intestine cadherin and its correlation with lymph node metastasis in gastric cancer: can it predict N stage preoperatively? Ann Surg Oncol 2007; 14: 94-99.

[40] Liu LX, Lee NP, Chan VW, Xue W, Zender L, Zhang C, Mao M, Dai H, Wang XL, Xu MZ, Lee TK, Ng IO, Chen Y, Kung HF, Lowe SW, Poon RT, Wang JH and Luk JM. Targeting cadherin-17 inactivates Wnt signaling and inhibits tumor growth in liver carcinoma. Hepatology 2009; 50: 1453-1463.

[41] Jin Y, Huang Y, Ren H, Huang H, Lai C, Wang W, Tong Z, Zhang H, Wu W, Liu C, Bao X, Fang W, Li H, Zhao P and Dai X. Nano-enhanced immunotherapy: targeting the immunosuppressive tumor microenvironment. Biomaterials 2024; 305: 122463.

[42] Zheng H, Chen X, Li Q, Liu Y and Cai J. Effects of chemotherapy and immunotherapy on microbial diversity in TME and engineered bacterial-mediated tumor therapy. Front Immunol 2023; 14: 1084926.

[43] Pavlova NN and Thompson CB. The emerging hallmarks of cancer metabolism. Cell Metab 2016; 23: 27-47.

[44] Liu Y, Zhao Y, Song H, Li Y, Liu Z, Ye Z, Zhao J, Wu Y, Tang J and Yao M. Metabolic reprogramming in tumor immune microenvironment: impact on immune cell function and therapeutic implications. Cancer Lett 2024; 597: 217076.

[45] Wang Z and Chen X. Establishment and validation of an immune-associated signature in

lung adenocarcinoma. Int Immunopharmacol 2020; 88: 106867.
[46] Chen S, Duan Y, Wu Y, Yang D and An J. A novel integrated metabolism-immunity gene expression model predicts the prognosis of lung adenocarcinoma patients. Front Pharmacol 2021; 12: 728368.
[47] Zhao S, Zhang H, Mu Q, Jiang Y, Zhao X, Wang K, Shi Y, Li X and Sun D. Integrative single-cell and machine learning analysis identifies a nucleotide metabolism-related signature predicting prognosis and immunotherapy response in LUAD. Cancers (Basel) 2026; 18: 160.
[48] Gu W, Wu Y, Jiang R, Shi M, Qi J and Lai J. A 12-gene immune signature predicts prognosis and identifies KRT6B as a therapeutic target in lung adenocarcinoma. Front Immunol 2026; 17: 1693469.
[49] Leveque E, Rouch A, Syrykh C, Mazières J, Brouchet L, Valitutti S, Espinosa E and Lafouresse F. Phenotypic and histological distribution analysis identify mast cell heterogeneity in non-small cell lung cancer. Cancers (Basel) 2022; 14: 1394.
[50] Wang JB, Huang X and Li FR. Impaired dendritic cell functions in lung cancer: a review of recent advances and future perspectives. Cancer Commun (Lond) 2019; 39: 43.
[51] Yoneda K, Kuwata T, Kanayama M, Mori M, Kawanami T, Yatera K, Ohguri T, Hisaoka M, Nakayama T and Tanaka F. Alteration in tumoural PD-L1 expression and stromal CD8-positive tumour-infiltrating lymphocytes after concurrent chemo-radiotherapy for non-small cell lung cancer. Br J Cancer 2019; 121: 490-496.
[52] McGranahan N, Rosenthal R, Hiley CT, Rowan AJ, Watkins TBK, Wilson GA, Birkbak NJ, Veeriah S, Van Loo P, Herrero J and Swanton C; TRACERx Consortium. Allele-specific HLA loss and immune escape in lung cancer evolution. Cell 2017; 171: 1259-1271.
[53] Bremnes RM, Al-Shibli K, Donnem T, Sirera R, Al-Saad S, Andersen S, Stenvold H, Camps C and Busund LT. The role of tumor-infiltrating immune cells and chronic inflammation at the tumor site on cancer development, progression, and prognosis: emphasis on non small cell lung cancer. J Thorac Oncol 2011; 6: 824-833.
[54] Barkal AA, Weiskopf K, Kao KS, Gordon SR, Rosental B, Yiu YY, George BM, Markovic M, Ring NG, Tsai JM, McKenna KM, Ho PY, Cheng RZ, Chen JY, Barkal LJ, Ring AM, Weissman IL and Maute RL. Engagement of MHC class I by the inhibitory receptor LILRB1 suppresses macrophages and is a target of cancer immunotherapy. Nat Immunol 2018; 19: 76-84.
[55] Bagchi S, Yuan R and Engleman EG. Immune Checkpoint Inhibitors for the treatment of cancer: clinical impact and mechanisms of response and resistance. Annu Rev Pathol 2021; 16: 223-249.
[56] Patel SP, Othus M, Chae YK, Azenkot T, Alviz C, Threlkel S, Haymaker C, Streicher HZ, Magner CM, Chen HX, Sharon E, Ryan CW, Blanke CD and Kurzrock R. DART (NCI/SWOG S1609): comprehensive final results from dual checkpoint inhibition with CTLA-4 and PD-1 blockade in rare cancers. Ann Oncol 2026; 37: 1167-1177.
[57] Rocha P, Bach R, Masfarré L, Hernandez S, Navarro-Gorro N, Rossell A, Villanueva X, Giner M, Sanchéz I, Galindo M, Del Rey-Vergara R, Iñañez A, Sanchéz-Espiridion B, Lu W, Acedo-Terrades A, Berenguer-Molins P, Sánchez-Font A, Chalela R, Curull V, Taus Á, Hardy-Werbin M, Sausen M, Georgiadis A, White J, Jackson JB, Moliner L, Clavé S, Bellosillo B, Rovira A, Wistuba I, Soto LMS, Perera-Bel J and Arriola E. Molecular and immunological features associated with long-term benefits in metastatic NSCLC patients undergoing immune checkpoint blockade. Oncoimmunology 2025; 14: 2469377.
[58] Liang F, Zhang S, Wang Q and Li W. Clinical benefit of immune checkpoint inhibitors approved by US food and drug administration. BMC Cancer 2020; 20: 823.
[59] Wojas-Krawczyk K, Kalinka E, Grenda A, Krawczyk P and Milanowski J. Beyond PD-L1 markers for lung cancer immunotherapy. Int J Mol Sci 2019; 20: 1915.
[60] Wu P, Wu D, Li L, Chai Y and Huang J. PD-L1 and survival in solid tumors: a meta-analysis. PLoS One 2015; 10: e0131403.
[61] Rojas-Diaz JM, Solorzano-Ibarra F, Garcia-Barrientos NT, Klimov-Kravtchenko K, Cruz-Ramos JA, Guitron-Aviña MS, Urciaga-Gutierrez PI, Ortiz-Lazareno PC, Tellez-Bañuelos MC, Bueno-Topete MR, Haramati J and Del Toro-Arreola S. Beyond canonical immune checkpoints: overexpression of TNFRSF members 4-1BB and OX-40 marks T cells exhibiting phenotypic features of exhaustion in cervical carcinoma. Immunology 2025; 175: 482-500.
[62] Zhou J, Yang Y, Ye R, Lin J, Feng H, Pei X, Li M, Peng J, Yang X, Woo PYM, Chan DTM, Zhou P, Mao J, Liu Z and Wu D. GITR activation potentiates anti-tumor immunity of tumor-infiltrating lymphocytes expanded from glioblastoma by rescuing exhaustion. Oncogene 2026; 45: 1087-1099.
[63] Zhang Y, Chen Y, Huang W, Zhou Y, Wang Y, Fu K and Zhuang W. NPAS2 dampens chemo-sensitivity of lung adenocarcinoma cells by en-

hancing DNA damage repair. Cell Death Dis 2024; 15: 101.
[64] Wang J, Liang J, Li H, Han J, Jiang J, Li Y, Feng Z, Zhao R and Tian H. Oncogenic role of abnormal spindle-like microcephaly-associated protein in lung adenocarcinoma. Int J Oncol 2021; 58: 23.
[65] Zheng Y, Sun B and Qu Z. Adverse predictive value of ASPM on lung adenocarcinoma overall survival depended on chemotherapy status. Future Sci OA 2025; 11: 2489328.
[66] Zhang W, Yu L, Xu C, Tang T, Cao J, Chen L, Pang X and Ren W. PLEK2 activates the PI3K/AKT signaling pathway to drive lung adenocarcinoma progression by upregulating SPC25. Cell Biol Int 2024; 48: 1285-1300.
[67] Chen P, Xiao L, Lv C, Zhang Q, Wu Y and Chen M. Multi-omics analysis links FERMT1 expression to patient survival, immunotherapy response, and metastasis across cancers. Transl Cancer Res 2026; 15: 21.
[68] Shi S, Luo D, Yang Y and Wang X. Integrative omics analysis reveals metabolic features of ground-glass opacity-associated lung cancer. J Cancer 2024; 15: 1848-1862.
[69] Chang W, Luo B, Wen Z and Chen Y. Harnessing machine learning-driven multiomics integration: deciphering programmed cell death networks for prognostication and immunotherapy prediction in lung adenocarcinoma. Cell Biol Toxicol 2026; 42: 17.
[70] Song D, Zhao L, Zhao G, Hao Q, Wu J, Ren H and Zhang B. Identification and validation of eight lysosomes-related genes signatures and correlation with immune cell infiltration in lung adenocarcinoma. Cancer Cell Int 2023; 23: 322.
[71] Wu D, Liu Y, Liu J, Ma L and Tong X. Myeloid cell differentiation-related gene signature for predicting clinical outcome, immune microenvironment, and treatment response in lung adenocarcinoma. Sci Rep 2024; 14: 17460.
[72] Bartolomé RA, Barderas R, Torres S, Fernandez-Aceñero MJ, Mendes M, García-Foncillas J, Lopez-Lucendo M and Casal JI. Cadherin-17 interacts with α2β1 integrin to regulate cell proliferation and adhesion in colorectal cancer cells causing liver metastasis. Oncogene 2014; 33: 1658-1669.
[73] Su MC, Yuan RH, Lin CY and Jeng YM. Cadherin-17 is a useful diagnostic marker for adenocarcinomas of the digestive system. Mod Pathol 2008; 21: 1379-1386.
[74] Lopes N, Bergsland C, Bruun J, Bjørnslett M, Vieira AF, Mesquita P, Pinto R, Gomes R, Cavadas B, Bennett E, Pereira L, Lothe RA, Almeida R and David L. A panel of intestinal differentiation markers (CDX2, GPA33, and LI-cadherin) identifies gastric cancer patients with favourable prognosis. Gastric Cancer 2020; 23: 811-823.
[75] Wang XQ, Luk JM, Garcia-Barcelo M, Miao X, Leung PP, Ho DW, Cheung ST, Lam BY, Cheung CK, Wong AS, Lau SS, So MT, Yu WC, Cai Q, Liu KS, Hui CK, Lau GK, Poon RT, Wong J and Fan ST. Liver intestine-cadherin (CDH17) haplotype is associated with increased risk of hepatocellular carcinoma. Clin Cancer Res 2006; 12: 5248-5252.
[76] Liu X, Huang Y, Yuan H, Qi X, Manjunath Y, Avella D, Kaifi JT, Miao Y, Li M, Jiang K and Li G. Disruption of oncogenic liver-intestine cadherin (CDH17) drives apoptotic pancreatic cancer death. Cancer Lett 2019; 454: 204-214.
[77] Panarelli NC, Yantiss RK, Yeh MM, Liu Y and Chen YT. Tissue-specific cadherin CDH17 is a useful marker of gastrointestinal adenocarcinomas with higher sensitivity than CDX2. Am J Clin Pathol 2012; 138: 211-222.
[78] Lee HJ, Nam KT, Park HS, Kim MA, Lafleur BJ, Aburatani H, Yang HK, Kim WH and Goldenring JR. Gene expression profiling of metaplastic lineages identifies CDH17 as a prognostic marker in early stage gastric cancer. Gastroenterology 2010; 139: 213-225, e213.
[79] Fernandez B, Lopez L, Matis T, Dabernat S and Amintas S. Cadherin 17 and digestive cancers: from diagnostic to therapeutic opportunities. J Exp Clin Cancer Res 2026; 45: 116.
[80] Zhang Z, Xiahou Z, Wu W and Song Y. Nitrogen metabolism disorder accelerates occurrence and development of lung adenocarcinoma: a bioinformatic analysis and in vitro experiments. Front Oncol 2022; 12: 916777.

Table S1. Analysis of clinicopathological features of LUAD in training cohort and in internal validation cohort

Characteristic	Training cohort (n = 448)	Internal validation cohort (n = 225)	*P*-value
Age			
< 65	200 (44.6%)	100 (44.4%)	
≥ 65	248 (55.4%)	125 (55.6%)	0.9610
Gender			
Female	246 (54.9%)	126 (56.0%)	
Male	202 (45.1%)	99 (44.0%)	0.7886
Stage			
Stage I	240 (53.5%)	120 (53.3%)	
Stage II	103 (23.0%)	52 (23.1%)	
Stage III	73 (16.3%)	37 (16.5%)	
Stage IV	24 (5.4%)	12 (5.3%)	
Unknown	8 (1.8%)	4 (1.8%)	> 0.9999
T			
T1	153 (34.1%)	83 (36.9%)	
T2	237 (52.9%)	116 (51.6%)	
T3	37 (8.3%)	14 (6.2%)	
T4	18 (4.0%)	9 (4.0%)	
Unknown	3 (0.7%)	3 (1.3%)	0.7283
M			
M0	299 (66.7%)	144 (64.0%)	
M1	23 (5.2%)	11 (4.9%)	
Unknown	126 (28.1%)	70 (31.1%)	0.7235
N			
N0	288 (64.3%)	142 (63.1%)	
N1	84 (18.8%)	44 (19.6%)	
N2	63 (14.1%)	33 (14.7%)	
N3	2 (0.4%)	1 (0.4%)	
Unknown	11 (2.4%)	5 (2.2%)	0.9943

LUAD, lung adenocarcinoma.

Table S2. 30 differentially expressed IMRGs related to prognosis in LUAD patients

Gene	HR	HR.95L	HR.95H	*P*-value
CACNA2D2	0.832577	0.746949	0.928022	0.000936
CYP24A1	1.085004	1.003847	1.172722	0.039710
HSD17B6	0.841320	0.747380	0.947067	0.004233
STYK1	1.286765	1.063839	1.556404	0.009390
COL11A1	1.100891	1.016679	1.192078	0.017915
MCM10	1.169218	1.019054	1.341510	0.025808
ASPM	1.314626	1.141023	1.514641	0.000153
CLDN18	0.910428	0.834016	0.993842	0.035899
MAOB	0.832654	0.734772	0.943576	0.004102
HMMR	1.469443	1.230419	1.754901	0.000022
SPAG5	1.248202	1.056627	1.474512	0.009110
LAMP3	0.884605	0.793084	0.986687	0.027773
CDH17	1.155321	1.064095	1.254368	0.000581
NDC80	1.218903	1.084510	1.369949	0.000897
ORC1	1.233553	1.035872	1.468960	0.018500
AURKA	1.270408	1.082668	1.490704	0.003352
CASS4	0.695055	0.547536	0.882319	0.002803
TPX2	1.250943	1.098070	1.425100	0.000761
BIRC5	1.268233	1.091125	1.474088	0.001959
KIF4A	1.343293	1.144763	1.576253	0.000298
CLSPN	1.248386	1.045580	1.490529	0.014177
CDC45	1.127638	1.012805	1.255490	0.028369
CDC6	1.224655	1.037116	1.446106	0.016862
CRTAC1	0.768702	0.667941	0.884663	0.000243
PGC	0.942672	0.893565	0.994478	0.030555
PLA2G3	0.776585	0.629509	0.958024	0.018262
BIK	1.177330	1.027370	1.349179	0.018854
PLEK2	1.467289	1.245310	1.728836	0.000005
MYBL2	1.130845	1.014475	1.260564	0.026463
FERMT1	1.281553	1.091067	1.505295	0.002515

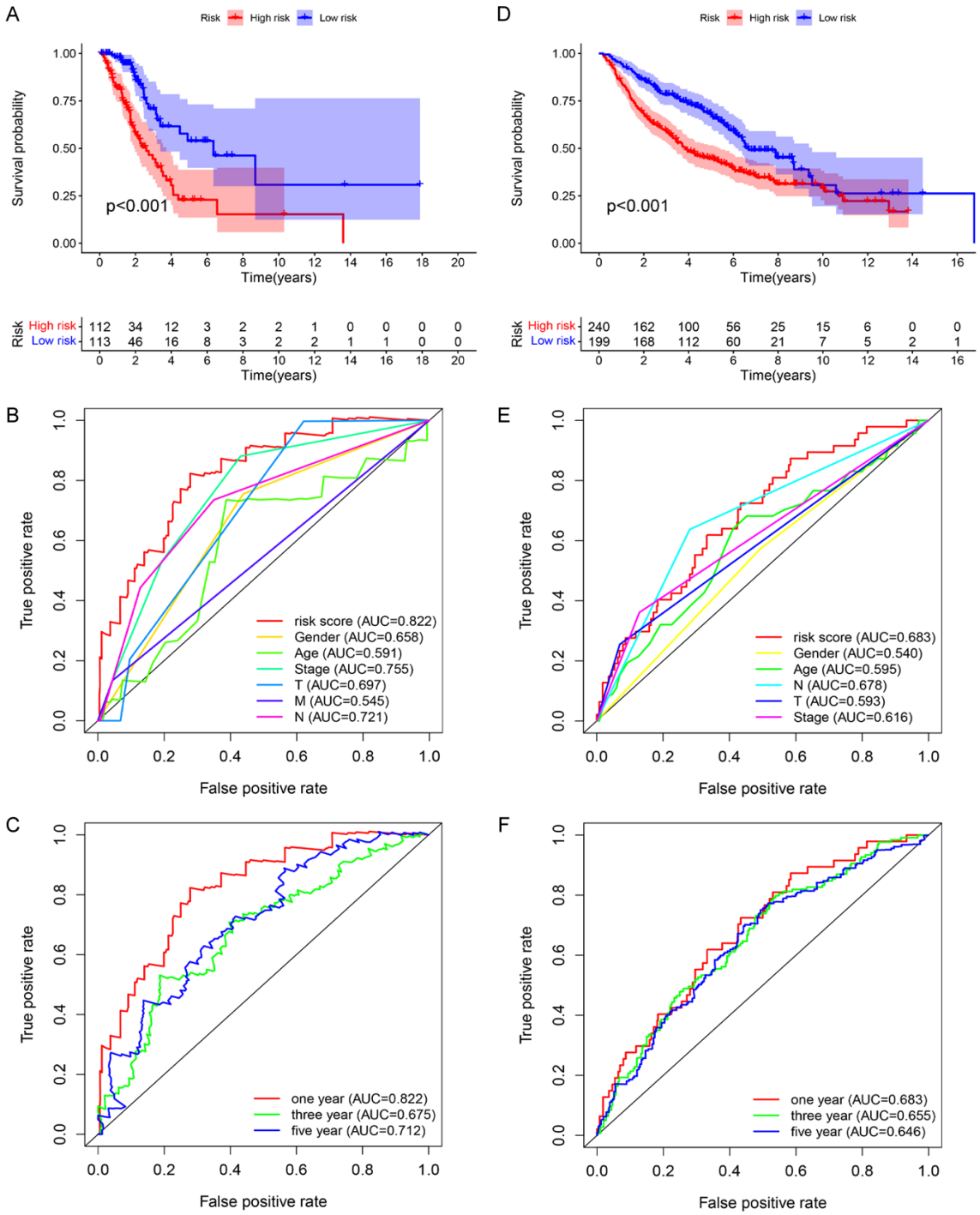


Figure S1. Prognostic value of IMRGs signature in the internal validation cohort and external validation cohort. A, D. Kaplan-Meier survival curves of OS between LR and HR groups in the internal validation cohort and external validation cohort, respectively; B, E. Comparing the AUC of the risk scores with other clinical parameters in the internal validation cohort and external validation cohort, respectively; C, F. Time-dependent ROC analysis of risk scores for predicting the OS in the internal validation cohort and external validation cohort, respectively. OS, overall survival; LR, low-risk; HR, high-risk; AUC, area under the curve; ROC, receiver operating characteristic.

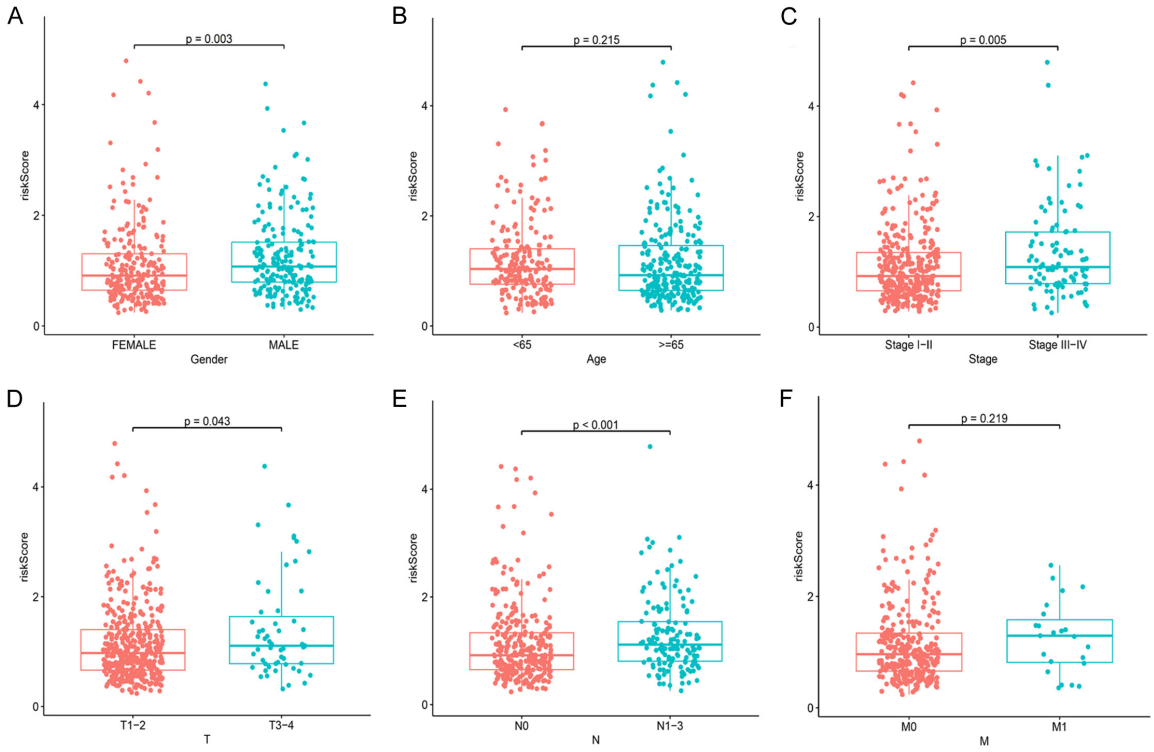


Figure S2. Correlation between IMRGs risk score and clinical typing. A. Gender; B. Age; C. Stage; D. T; E. N; F. M. IMRGs, immune- and metabolism-related genes.

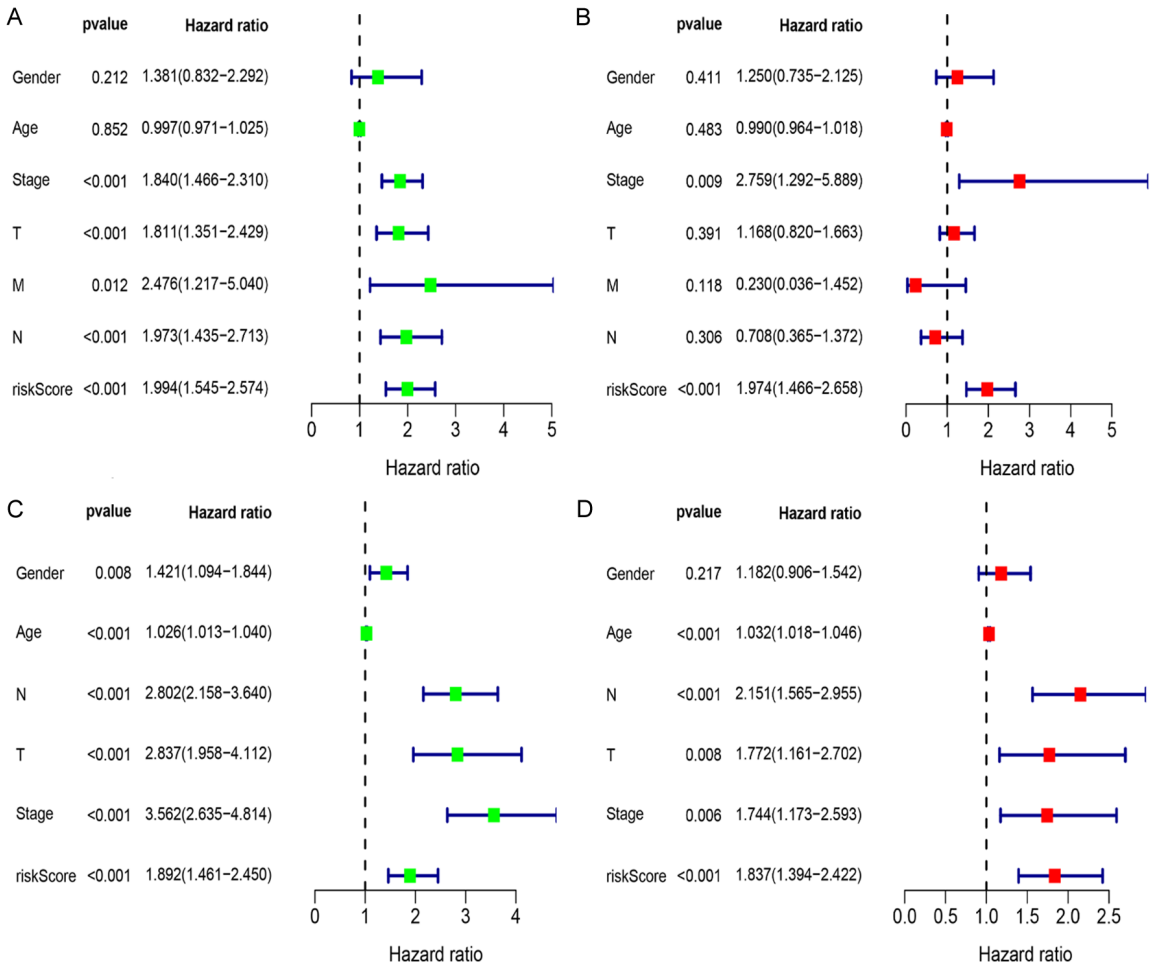


Figure S3. Univariate and multivariate Cox regression analyses of risk score and various clinical features in the internal validation cohort (A, B) and in the external validation cohort (C, D).

Table S3. Positively and negatively enriched biological functions and pathways of the IMRGs signature by GSEA

Gene set	Regulation	Pathway name	NES	NOM *p*-value	FDR q-value
GO	positive	mitotic nuclear division	2.48	< 0.001	< 0.001
GO	positive	microtubule cytoskeleton organization involved in mitosis	2.44	< 0.001	< 0.001
GO	positive	organelle fission	2.43	< 0.001	< 0.001
GO	positive	chromosome localization	2.43	< 0.001	< 0.001
GO	positive	condensed chromosome	2.35	< 0.001	< 0.001
GO	negative	lipid oxidation	-2.09	< 0.001	0.147
GO	negative	complement activation	-2.05	< 0.001	0.206
GO	negative	transcytosis	-2.05	0.004	0.200
GO	negative	regulation of lipopolysaccharide mediated signaling pathway	-2.03	0.002	0.204
GO	negative	regulation of fatty acid oxidation	-2.01	< 0.001	0.160
KEGG	positive	cell cycle	2.38	< 0.001	< 0.001
KEGG	positive	pyrimidine metabolism	2.29	< 0.001	0.001
KEGG	positive	oocyte meiosis	2.22	< 0.001	0.001
KEGG	positive	nucleotide excision repair	2.17	< 0.001	0.002
KEGG	positive	proteasome	2.16	< 0.001	0.002
KEGG	negative	fatty acid metabolism	-1.85	0.005	0.100
KEGG	negative	PPAR signaling pathway	-1.84	0.002	0.086
KEGG	negative	glycerophospholipid metabolism	-1.82	0.002	0.075
KEGG	negative	histidine metabolism	-1.83	0.002	0.086
KEGG	negative	tryptophan metabolism	-1.78	0.009	0.080

GSEA, Gene Set Enrichment Analysis; NES, normalized enrichment score; NOM, nominal; FDR, False Discovery Rate; GO, Gene Ontology; KEGG, Kyoto Encyclopedia of Genes and Genomes.